Article:
Yang, D., Liu, F., Huang, S.-S. et al. (2021) Structural fire safety design of square and rectangular tubed-reinforced-concrete columns. Structures, 29. pp. 1286-1321. ISSN: 2352-0124

https://doi.org/10.1016/j.istruc.2020.12.014

Structural fire safety design of square and rectangular tubed-reinforced-concrete columns

Dongdong Yang [a,b], Faqi Liu [a,b,*], Shan-Shan Huang [c], Hua Yang [a,b]

[a] *Key Lab of Structures Dynamic Behaviour and Control (Harbin Institute of Technology), Ministry of Education, Heilongjiang, Harbin 150090, China*

[b] *Key Lab of Smart Prevention and Mitigation of Civil Engineering Disasters (Harbin Institute of Technology), Ministry of Industry and Information Technology, Heilongjiang, Harbin 150090, China*

[c] *Department of Civil and Structural Engineering, The University of Sheffield, Sir Frederick Mappin Building, Mappin Street, Sheffield S1 3JD, UK*

Abstract

The tubed-reinforced-concrete (TRC) columns have gained increasing use in the high-rise buildings and large-span stadiums in China, whereas the structural fire design method for square and rectangular TRC columns is still missing. Finite element analysis of the fire performance of square and rectangular TRC columns was conducted using a sequentially-coupled thermo-stress model. This model yielded good predictions against the experimental results of square TRC columns. Fire tests on two rectangular TRC columns were also conducted and presented in this paper, to further calibrate the model. Parametric studies were then conducted, through which it was found that the fire resistance of square and rectangular TRC columns decreases with the increase of load ratio or slenderness ratio and increases as the sectional dimension enlarges. Sectional aspect ratio has a minor influence on the fire resistance of rectangular TRC columns. A practical design method was proposed, for the first time, to determine the fire resistance of square and rectangular TRC columns with or without fire protection. The buckling reduction coefficient could be determined by the EC3 buckling curve (c) or the JGJ/T471 buckling curve. The heat transfer equations given in the Japanese AIJ recommendation were modified to determine the temperatures of the steel tube and rebars and equations were proposed to determine the equivalent temperatures of the concrete core.

Keywords: Square and rectangular tubed-reinforced-concrete (TRC) columns; Fire resistance; Experiments; FEA; Design method; Fire protection.

1. Introduction

The concept of tubed-reinforced-concrete (TRC) columns, also known as steel tube confined reinforced concrete (STCRC) columns, came from the idea of replacing the dense stirrups in traditional reinforced concrete (RC) columns with thin steel hollow sections [1-2]. The steel tube of a TRC column is designed to mainly provide confinement to the concrete core without directly sustaining axial load by being terminated at the beam-column joint. This differs from the case of a concrete-filled steel tubular (CFST) column, whose steel tube sustains the axial force with the concrete together. The steel tube of a TRC column can be approximately considered as under pure tension stresses in the transverse direction and thus its confinement to the inner concrete is more effective than that in a CFST column. Since the steel tube of a TRC column is under very tiny axial compression, the risk of tube local buckling is minimised, therefore, much thinner steel tubes can be used. Over the past a few decades, the compressive and seismic performance of circular and square TRC columns have been investigated by various researchers [3-13]. Thanks to the composite actions between steel and concrete, TRC columns are found to possess advantages such as high strength, good ductility and favourable performance under cyclic loadings. The TRC columns have been increasingly used in engineering applications, i.e. high-rise buildings and large-span stadiums in China [14], and there is a Chinese technical standard JGJ/T471 for the design of TRC columns [15].

Fire accidents may cause great losses of lives and structural failures. The structural fire safety design is a key issue for steel-concrete composite columns. TRC columns behave differently in fire compared to the CFST columns due to the differences in the axial deformation behaviour and risk of steel tube local buckling. Though extensive studies have been conducted on the fire performance of CFST columns [16-23], the behaviour of TRC columns in fire is still not so understood. Liu et al. [24] developed a fire design method of circular TRC columns based on fire resistance tests and numerical studies. The research on the fire performance of square TRC columns is still limited and the authors have conducted an experimental study on five square TRC columns [25]. However, the research on the fire

performance of rectangular TRC columns, either experimental or numerical, has not been reported to the knowledge of the authors. The lack of the fire performance research of square and rectangular TRC columns is inconsistent with their current wide engineering applications. Therefore, there is a need for more fire research and structural fire safety design methods for square and rectangular TRC columns.

In this study, a 3-D nonlinear sequentially-coupled thermo-stress FEA model was built to analyse the fire performance of square and rectangular TRC columns. This model considers geometrical nonlinearity, material nonlinearity and complex contact behaviour at the concrete-steel interface. Following the previous experimental studies on four circular TRC columns [24] and five square TRC columns [25], fire tests on two rectangular TRC columns were conducted in this paper to calibrate the numerical model. The temperature profiles, column displacements, failure mode and fire resistance of the tested square and rectangular TRC columns could be well predicted by the FEA modelling. The influences of various parameters, such as load ratio, cross-section dimensions, slenderness ratio and sectional aspect ratio were investigated through parametric studies. Simplified design equations were recommended for the calculations of the temperature profiles within the cross-section of a square or rectangular TRC column. On the basis of the ambient-temperature design method of TRC columns given in JGJ/T471 [15], a high-temperature design method for the protected and unprotected square and rectangular TRC columns was proposed.

2. FEA modelling

A nonlinear 3-D FEA model based on the sequentially-coupled temperature-displacement modelling process in ABAQUS was previously built by the authors [25]. A heat transfer analysis was first conducted and its temperature outputs were then input into the stress analysis. The meshing details of the heat transfer model and stress analysis model are the same except for the element types. This FEA model was validated well against the standard fire tests of square TRC columns in [25] and is still used in this paper to carry out the modelling work of the performance of square and rectangular TRC columns in ISO 834 standard fire [26].

2.1 Heat transfer model

In accordance with EC1 [27], the convective coefficients 25 W/(m^2·K) and 9 W/(m^2·K) were adopted for the heated surface and unheated surface of the column, respectively. The emissivity coefficient of steel in fire may vary. The value (0.5) recommended by ECCS 1988 [28] is found suitable for the modelling of previous fire tests [24,25,29-33] that were conducted in the same gas furnace as for the tests modelled in this study. This value was also used by Han et al. [34-37], Ding and Wang [38], Yang and Fu [39] and Xu and Liu [40] in the thermal analysis of CFST columns. Therefore, the value of 0.5 is chosen for the thermal analysis of this study. The thermal resistance at the steel-concrete interface was considered in the model; a value of 100 W/(m^2·K) given by CIDECT [41], Ding and Wang [38] and Lv et al. [42], was adopted, which was assessed to be effective for the thermal analysis of circular and square TRC columns [24,25].

The nodes of rebar and concrete at the same location were tied together, assuming that their temperatures were identical. To achieve that, the concrete section was carefully partitioned at the locations of rebars. To obtain an accurate temperature distribution in the steel tube, nine integration points were set along its thickness direction. The temperature-dependent thermal conductivity, specific heat relationships proposed by Lie [43] for concrete and steel were adopted in this study. These thermal models have been validated by the research conducted by the authors [24,25,29-33] and other researchers [34,39,44-46]. The influence of water evaporation on heat transfer was considered by modifying the specific heat value of concrete at 100 °C using the method recommended by Han [16]. The moisture content of concrete was assumed to be 5% by weight, except that measured values were used when validating the model against experiments where moisture contents were provided.

2.2 Stress analysis model

Two solid steel plates were used to model the endplates of each column of the fire tests. The steel plate was tied to the corresponding concrete surface without any interaction with the steel tube. This approach was adopted here since the axial load was directly applied only to

the inner RC core in TRC columns. The steel plate was considered as a rigid body and its physical movement was represented by the corresponding reference point. General surface-to-surface contact was used for the steel-to-concrete interface with a tangential friction coefficient of 0.3. Finite sliding formulation was selected in order to accurately model the interface behaviour. The rebars were embedded into the concrete to consider deformation compatibility. A mesh sensitivity study was performed and there were general 12-20 elements along the column section edge to ensure the simulation accuracy.

The concrete damage plasticity (CDP) model of ABAQUS was used to model the high-temperature behaviour of concrete. The values of the following key parameters, i.e. dilation angle, flow potential eccentricity, the ratio of biaxial to uniaxial compressive strength, the stress invariant between the tensile and compressive meridians and viscosity parameter, given in reference [25] were used in the CDP model. The compressive stress-strain relationship of concrete proposed by Lie [43] (Eq. (1)) and the tensile constitutive model recommended by Hong and Varma [44] (Eq. (2)) were used. These stress-strain curves at different temperatures for concrete of cylinder compressive strength 40 MPa are shown in Fig. 1. The stress-strain models given in EC2 [47] and EC3 [48] were used to model the high-temperature behaviour of the rebars and steel tube, respectively. The initial overall imperfection of a column was taken as $L/1000$ (L is the column length) following the deflection shape of the first buckling mode.

$$\sigma_{cc,T}=\begin{cases} f_{cT}^{'}\left[1-\left(\dfrac{\varepsilon_{max}-\varepsilon_{cc,T}}{\varepsilon_{max}}\right)^2\right] & \varepsilon_{cc,T}\le\varepsilon_{max} \\ f_{cT}^{'}\left[1-\left(\dfrac{\varepsilon_{cc,T}-\varepsilon_{max}}{3\varepsilon_{max}}\right)^2\right] & \varepsilon_{cc,T}>\varepsilon_{max} \end{cases} \tag{1}$$

where $f_{cT}^{'}=\begin{cases} f_c^{'} & 0°C<T<450°C \\ f_c^{'}\left[2.011-2.353\left(\dfrac{T-20}{1000}\right)\right] & 450°C\le T\le 874°C \\ 0 & T>874°C \end{cases}$, $f_c^{'}$ is the cylinder compressive strength of concrete at room temperature, $\varepsilon_{max}=0.0025+(6T+0.04T^2)\times10^{-6}$.

$$\sigma_{ct,T}=\begin{cases} E_{cT}\varepsilon_{ct,T} & \varepsilon_{ct,T}\le\varepsilon_{cr} \\ f_{tT}^{'}-0.1f_{tT}^{'}\dfrac{\varepsilon_{ct,T}-\varepsilon_{cr}}{\varepsilon_{cr}} & \varepsilon_{cr}<\varepsilon_{ct,T}\le 2\varepsilon_{cr} \\ 0.9f_{tT}^{'} & \varepsilon_{ct,T}>2\varepsilon_{cr} \end{cases} \quad (2)$$

where $f_{tT}^{'}=0.09f_{cT}^{'}$, $\varepsilon_{cr}=f_{tT}^{'}/E_{cT}$.

3. Validation of FEA modelling against experiments

3.1 Rectangular TRC columns

3.1.1 Experiment description

Further testing on two slender rectangular TRC columns is presented here and used to further validate the FEA model described in Section 2. These two columns were named as TRC-0.5-1.5 and TRC-0.5-2, where 0.5 is the value of load ratio n ($n = N_f/N_b$, N_f is the applied constant axial load in fire and N_b is the buckling capacity according to JGJ/T471 [15]), 1.5 or 2 represents the sectional aspect ratio k ($k = D/B$, D and B are the sectional depth and width). Other details of these two columns, including the steel tube thickness t_s, sectional steel ratio α_s ($\alpha_s = A_s/A_c$, A_s and A_c are the sectional areas of steel tube and concrete, respectively) and reinforcement ratio ρ ($\rho = A_b/A_c$, A_b is the sectional area of reinforcement bars) are listed in Table 1.

A schematic of the test setup is shown in Fig. 2(a). The reinforcement arrangements in these two specimens are illustrated in Figs. 2(b) and 2(d). The concrete cover was 25 mm. The diameters and spacing of stirrups in these two rectangular columns were the same as those in the square columns described in [25].

Type K thermocouples were used to measure the temperature-time histories of the columns; the locations of the thermocouples are shown in Figs. 2(c) and 2(e) by red dots. For the specimen TRC-0.5-1.5, thermocouples 1 and 6 were welded to the tube surface, thermocouples 8-9 were fixed to the rebars and the other thermocouples were embedded in the concrete core. For TRC-0.5-2, thermocouples 1 and 7 were welded to the tube surface, thermocouples 9-10 measured the reinforcement temperatures, and the other thermocouples

were inside the concrete.

Self-compacting concrete (SCC) was used to cast the test specimens and the mix design was described in [25]. The cube compressive strengths of concrete f_{cu} were 31.9 MPa and 50.9 MPa on 28 days and on the day of testing (190 days), respectively. The concrete elastic modulus E_c on the day of testing was 38800 MPa. The moisture content was measured from three 100 mm cubes on the testing day following ISO 12570 [49] and the mean value was 5.4%. Mild steel was used for the steel tubes and rebars in the TRC columns. The material properties of steel tubes and rebars were obtained from coupon tests, whose results were included in Table 2, including the tube yield strength f_y, rebar yield strength f_b, ultimate strength f_u, elastic modulus E_s or E_b and Poisson's ratio v.

The columns were 3810 mm long and heated in a gas furnace, whose details were described in [24,25]. Each column was divided into three parts, by cutting two 30 mm gaps near column ends and only the 3000 mm middle part was directly exposed to fire. The axial load N_f is concentrically applied on to the column top end and then maintained constant during heating. The measured axial loads throughout the fire testing are shown in Figs. 3(a) and 3(b). The discrepancy between the measured and nominal values is generally within ± 3%, showing an acceptable level of loading control. The end boundary condition of TRC-0.5-1.5 was designed to be pinned about the major axis (y-axis in Fig. 2(b)); the corresponding slenderness ratio λ_D ($\lambda_D = 2\sqrt{3}L/D$) was 52.8. The end boundary condition of TRC-0.5-2 was designed to allow only minor axis (x-axis in Fig. 2(d)) rotation; the corresponding slenderness ratio λ_B ($\lambda_B = 2\sqrt{3}L/B$) was 105.6. Ten LVDTs were used to measure the axial and lateral displacements of each column; their detailed arrangements were the same as those in previous testing [25].

Eight thermocouples T1-T8 were placed in various locations inside the furnace to check the temperature uniformity within the furnace. Figs. 3(c)-3(e) present the measured furnace air temperature-time curves of these two tested columns. The temperature distribution in the furnace was uniform and followed well the ISO 834 standard fire, as designed. The average of these eight thermocouple measurements was defined as the furnace air temperature. The temperature evolutions of the columns are displayed in Fig. 4. The distance between a

measuring point and the perimeter of the concrete core is named as *d*. To minimize the influence of the flame on the steel tube temperature measurements, thermal insulating materials were used to locally cover the measurement points. Fig. 4(g) shows that the two steel tube temperature curves (Points 1 and 7) are slightly different from each other. It is speculated that the thermal insulations on the thermocouples may be slightly misplaced. At the same distance *d* from the perimeter of the concrete core, the thermocouples along the major axis of the rectangular section measured lower temperatures than those on the minor axis, as shown in Figs. 4(c) and 4(i).

The measured axial deformations *u* of these two specimens and the calculated deformation rates are shown in Figs. 5(a) and 5(b). These two columns experienced deformation runaway failure. The failure is defined as the axial deformation rate reaching the limit given in ISO 834-1 [26], which is 0.003*L* mm/min. The failure time is used to define the fire resistance $t_{FR,t}$, which is highlighted as a red dot in Figs. 5(a)-5(b). Specimen TRC-0.5-1.5 experienced contraction before failure, whereas specimen TRC-0.5-2 failed after considerate elongation. Fig. 5(c) plots the lateral deformation *w*-time curve of TRC-0.5-1.5 and this deformation is along the major axis bending direction; the lateral deformation data of TRC-0.5-2 is missing due to a malfunction of the testing equipment. The rotations *r* of the column top ends were derived from the axial deformations of the columns; the detailed formulations were given in [25] and thus not duplicated here. The rotation-time relations are shown in Fig. 5(d). Column TRC-0.5-2 experienced only minor axis rotation, which was smaller than that of TRC-0.5-1.5. This was possibly caused by the fact that TRC-0.5-2 was subject to a smaller applied load than that of TRC-0.5-1.5.

Both TRC-0.5-1.5 and TRC-0.5-2 experienced global buckling, together with tube local buckling of the steel tubes, as presented in Fig. 6. The steel tubes were removed to examine the concrete cores and rebars after testing, as illustrated in Fig. 7. The maximum residual lateral deformation of TRC-0.5-1.5 occurred at around 1.4 m from the top endplate, where the concrete was crushed and the reinforcements buckled with some of the rebars even fractured. Concrete cracking was found in the tension zone of this specimen. The column TRC-0.5-2 experienced the maximum residual lateral deformation at around 1.85 m from the top

endplate and the corresponding deformation was 100 mm. The measured residual column end rotations of TRC-0.5-2 were 3.5 ° and 3.7 ° for the top and bottom ends, respectively. No visible buckling of the longitudinal rebars was found. Transverse cracking throughout the whole cross-section in the tension zone was also observed.

The top end of TRC-0.5-1.5 was found to rotate about both the major and minor axes of the section, as it was impossible to apply 100% fixity to the minor axis bending at column top end where the load jack located. This led to a two-way flexural buckling deformation of TRC-0.5-1.5, as shown in Figs. 6 and 7. This buckling mode could be seen as the superposition of the following two modes: (a) buckling when both ends were allowed to rotate only about the major axis; (b) buckling when the column top was allowed to only rotate about the minor axis and the bottom end was fixed. The ambient-temperature buckling resistances of these two buckling modes are similar. The buckling resistance of mode (a) is 2437 kN and that of mode (b) is 2324 kN. This causes the two-way buckling failure of this specimen. In the fire tests on eccentrically-loaded rectangular CFST columns that were reported by Espinos et al [50], for some of the columns with moderated eccentricity (load eccentricity/sectional width = 0.2) that were designed to rotate only about their major axes, significant curvatures of the column in both planes were also observed. Thus, this two-way buckling deformation may be a concern for fire tests on rectangular columns that are designed only to bend about the major axis.

As noted above, the failure locations of these two specimens are different. In particular, TRC-0.5-1.5 fails at 1.4 m from the top endplate and TRC-0.5-2 fails at 1.85 m from the top endplate. This is mainly because the difference between the top and bottom boundary conditions varies in between these two cases. The column top end support is weaker than the bottom end support, since the top end may rotate about two directions, whereas the bottom end could rotate only about one direction, leading to two buckling modes. The difference between the buckling resistances of these two buckling modes of TRC-0.5-1.5 is less than that of TRC-0.5-2, and so the difference between the top and bottom boundary conditions is more significant in TRC-0.5-1.5 than in TRC-0.5-2. Therefore, TRC-0.5-1.5 fails close to the top end and TRC-0.5-2 fails at around the mid-height.

3.1.2 Validation of FEA modelling

The test results of these two rectangular TRC columns were used to verify the FEA models. The simulated temperature-time curves versus the measured results are shown in Fig. 4. A good agreement was achieved, especially for the temperatures of the steel tubes and rebars. Due to the complexity of the concrete high-temperature thermal properties and that the moisture migration was not considered in the thermal analysis, the measured temperature plateau of the concrete core at around 100 °C-150 °C couldn't be modelled by the thermal analysis. In general, the heat transfer analysis could give a reasonable prediction of the temperature evolutions of the rectangular TRC column sections.

As discussed in reference [25], it is difficult to achieve ideal pined-ended boundary conditions during testing due to the limitations of the loading device, such as non-negligible friction. To ensure the model represents the tests as much as possible, the measured column end rotations, as shown in Fig. 5(d), could be adopted in the stress analysis as boundary conditions. This approach has been validated and described in [25] and [51]. A sensitivity study has been carried out to identify the appropriate imperfection to be used in FEA to simulate the two-way buckling of TRC-0.5-1.5. Fig. 8 shows that the variation of the imperfection (from 1/500 to 1/5000) has a very little effect on the predicted axial and lateral deformations. Therefore, 1/1000 is applied to both the major- and minor-axis buckling. Figs. 5(e) and 5(f) show the FEA predicted axial deformation-time curves of three different boundary condition cases, i.e. measured rotation-time relationship $r(t)$, pinned-pinned and fixed-fixed. When using the measured rotational restraint $r(t)$ as the boundary condition, the predicted and measured axial deformation-time relationships match well with each other. The FEA results of the two idealised boundary conditions are considerably different from the measured result, indicating the significant impact of the rotational end restraint. Fig. 5(c) shows the simulated lateral deformation of TRC-0.5-1.5 and a good prediction was obtained compared with the test results. The FEA predicted failure modes were compared with the test results in Fig. 6. The bidirectional-curvature of the deformation shape of TRC-0.5-1.5 was also accurately predicted by the FEA.

3.2 CFST and RC columns

The heat transfer and mechanical behaviour of TRC columns in fire are closely affected by three interacting components, i.e. steel tube, concrete core and reinforcing bars, which is similar to the case of CFST columns. Since there are very few fire tests on TRC columns [24,25], fire tests on CFST columns are also used to validate the FEA models.

Fire tests on CFST columns conducted by other researchers, i.e. Lie and Chabot [52-53], Han et al. [54] and Espinos et al. [50,55] were used to further validate the heat transfer and mechanical FEA models. These test results include square and rectangular CFST columns, filled with plain or bar-reinforced concrete, with or without fire protection. The boundary conditions of these fire tests include pined-pined, fixed-fixed, and pined-fixed. The details of these test specimens are summarised in Table 3.

The heat transfer model of CFST columns is the same as that of TRC columns. For the protected CFST columns, the fire protection was modelled using the DC3D8 element of ABAQUS. Its inner surface was tied to the outer surface of steel tube. The fire protection thermal properties, reported alongside the test data [54] used for this validation, were adopted. The measured furnace temperature curves of the tests were employed in the FEA. Fig. 9 shows the typical comparison results of the FEA predicted temperature-time curves with the experimental results. A good agreement was achieved in general.

In the stress analysis of CFST columns, the steel tube was connected to endplates via shell-to-solid coupling and the endplates interacted with the concrete core via hard contact in the direction normal to the endplates. This setting is to account for the fact that, during the initial heating, the steel tube of a CFST column may expand more than the concrete and detach from the latter in the axial direction, as pointed by Espinos et al. [56]. Typical axial deformation-time curves predicted by the FEA are compared with test data in Fig. 10. The comparison indicates that the model could predict well the deformation behaviour of the CFST columns in fire.

26 fire tests on RC columns conducted by Lie and Woollerton [57] and Hass [58] of the following features (test duration < five hours, specimen cross section being square or rectangular, under concentric loading and with idealised boundary conditions) are selected to

further validate the FEA model. The predicted fire resistances $t_{FR,p}$ of these columns are compared with the test data $t_{FR,t}$ in Table 3. The mean value of $t_{FR,p}/t_{FR,t}$ is 0.91 and the standard deviation is 0.11. Figs. 10(g) and 10(h) show the comparison between the experimental and numerical axial deformation-time curves of four example specimens.

The FEA predicted fire resistance $t_{FR,p}$ are compared with the experimental one $t_{FR,t}$ from the collected results of CFST and RC columns in Table 3. The mean value of $t_{FR,p}/t_{FR,t}$ is 0.97 with a standard deviation of 0.12. Considering the relatively high variability of fire test results, these FEA models can reasonably predict the thermal and mechanical responses of both TRC and CFST columns in fire.

4. Parametric studies

4.1 Investigated parameters

The FEA models described in Section 2 were used to conduct parametric studies on the fire resistance of square and rectangular TRC columns. The investigated parameters include the load ratio n, sectional width of the square section or depth (dimension of the minor axis) of the rectangular section D, slenderness ratio λ, cube compressive strength of concrete f_{cu}, steel tube yield strength f_y, rebar yield strength f_b, steel ratio α_s, reinforcement ratio ρ and sectional aspect ratio k, as listed in Table 4. The concrete cover is 25 mm. All the columns were of the pined-ended boundary conditions and exposed to ISO 834 standard fire.

4.2 Results and discussions

Fig. 11 shows the influences of various parameters on the fire resistance of square TRC columns. Generally, the load ratio, slenderness ratio and sectional dimension are the three most influential parameters. The fire resistance decreases as load ratio or slenderness ratio increases, whereas larger sectional dimensions lead to higher fire resistance. This was also seen from circular TRC columns [24] and CFST columns [50,52-55]. An increase in concrete compressive strength is beneficial for the enhancement of fire resistance. The rebars' temperatures remain relatively low during heating and so their strength and stiffness

degradations are slight. Therefore, an increase in rebar strength or reinforcement ratio is beneficial in retaining the column capacity in fire and thus increases the column fire resistance. TRC columns with higher steel tube strength or higher steel ratio have lower fire resistance. This is because that higher steel tube strength or steel ratio results in higher confinement to the inner concrete at ambient temperature. However, during heating, the steel tube properties degrade very fast, leading to the rapid decrease of the column capacity. For columns with $n \leqslant 0.5$, $\lambda \leqslant 30$ and $D \geqslant 400$ mm, the fire resistance could reach 3 hours without passive fire protection, demonstrating the excellent fire performance of square TRC columns.

There is not yet a design method to determine the ambient-temperature load-bearing capacity of a rectangular TRC column. JGJ/T471 [15] provides guidance on the design of square TRC columns and suggests to (i) for aspect ratios smaller than 1.1, convert the rectangular TRC column to an equivalent square section of the same sectional area and steel ratio; (ii) for aspect ratios larger than 1.1, ignore the confinement of the steel tube to the concrete core. The effects of sectional aspect ratio on the ambient-temperature buckling resistance and fire resistance of rectangular TRC columns were investigated by FEA modelling. The rectangular columns with different aspect ratios were of the same sectional area D_{eq}^2, where D_{eq} is the width of the square column and $D_{eq} = (D \cdot B)^{1/2}$. All these rectangular TRC columns were designated to bend along their major axes. Sectional aspect ratio is found to have a very slight effect on the buckling resistance of the rectangular columns and the influence level is within only 1.7%. Fig. 12 shows the influence of sectional aspect ratio on the fire resistance of rectangular TRC columns, which is also marginal.

5. Structural fire safety design

A commonly-used fire safety design method for a composite column is to assess its high-temperature load-bearing capacity, as adopted in the Eurocode EC4 [59] and Chinese code GB 50936 [60]. As temperature increases, the column fails when its capacity falls below the applied axial load. In the FEA modelling described above, a transient heating analysis is adopted, where a constant load is applied then the column is heated till failure. The applied

constant load is then considered as the failure load at the corresponding fire resistance time.

5.1 Temperature profile

Since the heat transfer within a TRC section is the same as that of a CFST section in principle, the heat transfer formulations for square CFST columns given in the Japanese recommendation AIJ [61] were employed to calculate the temperatures of steel tube T_s and rebars T_b in square TRC columns, as shown in Eq. (3) and Eq. (4).

$$T_s = 1080 - 450\exp(-0.8t) - 630\exp(-3t) + 20 \tag{3}$$

where t is the heating time in hour.

$$T_b = (T_s - 20)\exp\left\{\left(\frac{13.5(2x/D_c - 1)}{(t/D_c^{\,2})^{3/4}}\right)\left(1 - 1.5\left(\frac{2y}{D_c}\right)^2\left(1 - \frac{2x}{D_c}\right)\right)\right\} + 20 \tag{4}$$

where D_c is the sectional dimension of concrete core in cm; x and y are the distances (in cm) between the calculated node and the two symmetric axes of the cross-section, of which x is the larger one, as illustrated in Fig. 13(a); and t is the heating time in second.

It should be noted that the influence of the steel tube temperature gradient on the temperature distribution within square CFST columns has been omitted in these AIJ equations (Eq. (3) and Eq. (4)). To assess the extent of the steel tube temperature gradient, a concrete filled tube of 600 mm width and 26mm wall thickness is analysed with FEA. The steel tube thickness is taken as the maximum steel tube to concrete area ratio (20%) for CFST columns given by Chinese code GB 50936 [60]. Fig. 14 shows that the steel tube thermal gradient is very little and so the AIJ equations, which has been developed for CFST columns with relatively thick tubes, should still be valid for TRC columns of very thin steel tubes.

Previous test results [25] and some of the FEA modelling results were used to verify these formulations, as shown in Fig. 15. These two equations could generally give good temperature predictions for the steel tube and reinforcements in square TRC sections. It should be noted that these formulae were especially proposed for square composite sections and their applicability for rectangular sections is still questionable. Eq. (3) was applied directly to calculate the steel tube temperature in rectangular TRC sections. For the reinforcements, Eq. (4) was modified for rectangular sections, as shown in Eq. (5). Eq. (3)

and Eq. (5) yield good temperature predictions for steel tube and reinforcement bars in rectangular composite sections, as shown in Fig. 16. Compared to the temperatures of steel tube and corner rebars, the temperatures of the middle rebars are lower and more affected by the surrounding concrete temperature and so experience a more obvious temperature plateau at around 100-150 °C, as shown in Fig. 16 (c). Since Eq. (5) does not account for this plateau, the discrepancy between test and predicted results is the most to middle rebars.

$$T_b = (T_s - 20)\exp\left\{\left(\frac{13.5(2x/D_1 - 1)}{(t/D_t^2)^{3/4}}\right)\left(1 - 1.5\left(\frac{2y}{D_2}\right)^2\left(1 - \frac{2x}{D_1}\right)\right)\right\} + 20 \quad (5)$$

where D_1 and D_2 (both in cm) are the sectional dimensions of the concrete core in the x and y directions, respectively, as illustrated in Figs. 13(b) and 13(c); If $y = 0$, $D_t = D_1$; otherwise $D_t = (D_1+D_2)/2$.

Due to the thermal properties of concrete, e.g. low thermal conductivity and high specific heat, apparent temperature gradients generally occur throughout the concrete core. As described in EC2 [47] and EC4 [59], to calculate the high-temperature capacity of an RC column or a CFST column, the concrete section is subdivided into several zones of equal thickness. The temperature, strength, and modulus of elasticity are assumed to be uniform within each zone. The load-bearing capacity of the cross-section is the sum of the capacity of each zone. However, this approach is time-consuming. Based on strength equivalence, the concepts of equivalent temperature and equivalent strength of the entire concrete section were proposed for circular TRC columns [24].

Similarly, for square TRC columns, the equivalent strength reduction factor k_{cfT} was derived from the FEA and then the equivalent strength temperature $T_{cf,eq}$ was obtained via an inverse calculation based on the strength reduction-temperature relationship given in [43]. The results of k_{cfT} and $T_{cf,eq}$ are plotted in Figs. 17(a) and 17(b). Simplified formulae Eq. (6) and Eq. (7) were previously proposed for k_{cfT} and $T_{cf,eq}$ of circular columns, based on regression analysis [24]. These formulae are also valid for square sections, on the basis that the cross-section shape does not influence the section factor as long as the sectional dimension is the same [62]. For rectangular columns, it is found that sectional aspect ratio has little influence on the equivalent strength reduction, as shown in Figs. 18(a)-18(d). This might be because that when

the columns' volumes remain the same with only the aspect ratios varying, the heat absorption capacities of the concrete sections are the same. Thus, Eq. (6) and Eq. (7) are also applicable for rectangular sections. These formulae have been verified against FEA modelling, indicating a reasonable match, as shown in Figs. 19(a) and 19(b).

$$k_{\mathrm{cfT}} = 1 - (\frac{0.045}{D_{\mathrm{c}}} - 0.016)t \tag{6}$$

$$T_{\mathrm{cf,eq}} = 449.7 + 425(\frac{0.045}{D_{\mathrm{c}}} - 0.016)t \tag{7}$$

where D_{c} (in m) is the equivalent sectional dimension of the inner concrete core; for square TRC columns, $D_{\mathrm{c}} = D\text{-}2t_{\mathrm{s}}$; for rectangular columns, $D_{\mathrm{c}} = (D \cdot B)^{1/2}\text{-}2t_{\mathrm{s}}$; t is the heating time in hour.

The equivalent elastic modulus of the whole concrete core of a TRC section $E_{\mathrm{c,eq},T}$ is defined as $E_{\mathrm{c,eq},T} = \dfrac{\sum_{\mathrm{i=1}}^{\mathrm{n_e}} E_{\mathrm{c,i},T} I_{\mathrm{ci}}}{I_{\mathrm{c}}}$, where $\mathrm{n_e}$ is the number of divided elements; $E_{\mathrm{c,i},T}$ is the high-temperature elastic modulus of concrete in element i; $E_{\mathrm{c,i},T} = 2f'_{\mathrm{c,i},T}/\varepsilon_{\mathrm{c,i},T}$; $f'_{\mathrm{c,i},T}$ and $\varepsilon_{\mathrm{c,i},T}$ are the concrete compressive strength and peak strain of element i, which is given in [43]; I_{ci} is the moment of inertia of element i along the section's central axis; and I_{c} is the moment of inertia of the whole concrete section. The equivalent stiffness reduction factor k_{cET} of concrete is expressed as $k_{\mathrm{cET}} = \dfrac{E_{\mathrm{c,eq},T}}{E_{\mathrm{c}}}$.

The evolutions over time of the equivalent stiffness reduction factors for square TRC columns are shown in Fig. 17(c). Compared with Fig. 17(a), it is found that the equivalent stiffness decreases faster than the equivalent strength as temperature rises. The influence of sectional aspect ratio on the equivalent stiffness reduction of rectangular sections is also found to be little, as presented in Figs. 18(e)-18(h).

As shown in Eq. (8), if k_{cfT} and k_{cET} are known, the equivalent stiffness temperature $T_{\mathrm{cE,eq}}$ can be determined. Fig. 17(d) shows the evolutions of $T_{\mathrm{cE,eq}}$ over heating time for various sectional dimensions.

$$k_{\mathrm{cET}} = \frac{2f'_{\mathrm{c},T}}{\varepsilon_{\mathrm{c},T}} / \frac{2f'_{\mathrm{c}}}{\varepsilon_{\mathrm{c}}} = k_{\mathrm{cfT}} \cdot \frac{2636}{2500 + (6T_{\mathrm{cE,eq}} + 0.04T^2_{\mathrm{cE,eq}})} \tag{8}$$

where $f_{\mathrm{c}}^{'}$ and ε_{c} are the cylinder compressive strength and peak strain of concrete at ambient temperature; $f_{\mathrm{c}}^{'},_T$ and $\varepsilon_{\mathrm{c},T}$ are the corresponding values at elevated temperature.

A regression equation is proposed for $T_{\mathrm{cE,eq}}$, as listed in Eq. (9).

$$T_{\mathrm{cE,eq}} = \frac{-9.8t^2 + 92.7t}{D_{\mathrm{c}}} + 20 \tag{9}$$

The calculated values of k_{cET} and $T_{\mathrm{cE,eq}}$ using the equations mentioned above agree well with FEA results, as shown in Figs. 19(c)-19(d).

5.2 Unprotected TRC columns

Eq. (10) was proposed to determine the compressive resistance $N_{\mathrm{u,T}}$ of a square TRC column at high temperature. This equation was adapted from the ambient-temperature design equation given in JGJ/T471 [15].

$$N_{\mathrm{u},T} = f_{\mathrm{cc},T}A_{\mathrm{c}} + f_{\mathrm{b},T}A_{\mathrm{b}} \tag{10}$$

where

$f_{\mathrm{b},T}$ is the high-temperature yield strength of reinforcement and $f_{\mathrm{b},T} = k_{\mathrm{bT}}f_{\mathrm{b}}$;

$f_{\mathrm{cc},T}$ is the high-temperature compressive strength of confined concrete and $f_{\mathrm{cc},T} = f_{\mathrm{c,eq},T} + 5.1f_{\mathrm{el},T}$;

$f_{\mathrm{c,eq},T}$ is the high-temperature equivalent compressive strength of the unconfined concrete and $f_{\mathrm{c,eq},T} = \beta k_{\mathrm{cfT}}f'_{\mathrm{c}}$;

$f_{\mathrm{el},T}$ is the high-temperature confinement stress from steel tube to inner concrete and $f_{\mathrm{el},T} = \dfrac{2k_{\mathrm{s},T}k_{\mathrm{h}}t_{\mathrm{s}}f_{\mathrm{y},T}}{D}$;

$f_{\mathrm{y},T}$ is the high-temperature yield strength of steel tube and $f_{\mathrm{y},T} = k_{\mathrm{yT}}f_{\mathrm{y}}$;

$k_{\mathrm{s},T}$ is the high-temperature reduction factor of confinement for a square TRC section and

$$k_{s,T}=\frac{27t_s}{D}\sqrt{\frac{f_{y,T}}{235}}\left(\frac{30}{f_{c,eq,T}}\right);$$

k_h is a reduction factor related to the steel tube transverse stress and $k_h = 0.75$;

k_{yT} and k_{bT} are the strength reduction factors of structural steel and reinforcement bars, respectively. A polynomial fitting curve Eq. (11) was proposed for determining k_{yT} and k_{bT} based on the tabulated values given in EC2 [47] and EC3 [48].

$$k_{yT} \text{ or } k_{bT}=\begin{cases}1 & 0.02\le T_n\le 0.4\\ 44.55T_n^5-186.48T_n^4+301.96T_n^3-232.73T_n^2+82.52T_n-9.78 & 0.4<T_n\le 1.1\\ -0.2T_n+0.24 & 1.1<T_n\le 1.2\end{cases} \quad (11)$$

$T_n = T/1000$

Differential thermal stresses exist in the concrete core due to the differential thermal expansions of different layers. The correction coefficient β was added to consider the negative effect of the differential thermal stresses on the column's resistance and β is given as $\frac{1}{1+(0.0054t+0.22)\sqrt{\frac{t}{D_c}}}$. As shown in Fig. 20(a), a better agreement was achieved after this correction.

The high-temperature buckling resistance $N_{b,T}$ of square TRC columns is the compressive resistance $N_{u,T}$ multiplied by the reduction coefficient φ_T, as shown in Eq. (12).

$$N_{b,T}=\varphi_T N_{u,T} \quad (12)$$

where φ_T is a function of the relative slenderness $\bar{\lambda}_T$ and $\bar{\lambda}_T=\sqrt{\frac{N_{u,T}}{N_{cr,T}}}$; $N_{cr,T}$ is the Euler buckling load at high temperature and $N_{cr,T}=\frac{\pi^2(EI)_{fi,eff}}{L_{eff}^2}$; L_{eff} is the effective column length; $(EI)_{fi,eff}=k_{sET}E_sI_s+k_{bET}E_bI_b+Ck_{cET}E_cI_c$; I_s and I_b are the second moments of area of steel tube and reinforcements, respectively; C is a parameter considering the sectional stiffness reduction of concrete and $C=0.6+2\frac{\alpha_s+\rho}{1+\alpha_s+\rho}\le 0.9$; k_{sET} and k_{bET} are the high-temperature elastic modulus reduction factors of structural steel and reinforcement bars, respectively. A regression formula Eq. (13) was given for k_{sET} and k_{bET} based on the tabulated values given in EC2 [47] and EC3

[48].

$$k_{\mathrm{sET}} \text{ or } k_{\mathrm{bET}} = \begin{cases} 1 & 0.02 \le T_{\mathrm{n}} \le 0.1 \\ -T_{\mathrm{n}} + 1.1 & 0.1 < T_{\mathrm{n}} \le 0.5 \\ 7.62T_{\mathrm{n}}^{4} - 31.17T_{\mathrm{n}}^{3} + 47.38T_{\mathrm{n}}^{2} - 31.93T_{\mathrm{n}} + 8.14 & 0.5 < T_{\mathrm{n}} \le 1.2 \end{cases} \tag{13}$$

$$T_n = T / 1000$$

The reduction coefficient φ_T in Eq. (12) can be determined either from the buckling curve (Eq. (14)) given in EC3 [63], or from the buckling curve (Eq. (15)) for square TRC columns given in JGJ/T471 [15].

$$\varphi_T = \frac{1}{\Phi + \sqrt{\Phi^2 - \bar{\lambda}_T^{\,2}}} \tag{14}$$

where $\Phi = 0.5[1 + \alpha(\bar{\lambda}_T - 0.2) + \bar{\lambda}_T^{\,2})$ and α is the imperfection factor.

$$\varphi_T = \begin{cases} 1 & \bar{\lambda}_T \le 0.15 \\ \left[1 + (1 + \varepsilon_1)/\bar{\lambda}_T^{\,2}\right]/2 - \sqrt{\left[1 + (1 + \varepsilon_1)/\bar{\lambda}_T^{\,2}\right]^2/4 - 1/\bar{\lambda}_T^{\,2}} & 0.15 \le \bar{\lambda}_T \le 1 \\ \left[1 + (1 + \varepsilon_2)/\bar{\lambda}_T^{\,2}\right]/2 - \sqrt{\left[1 + (1 + \varepsilon_2)/\bar{\lambda}_T^{\,2}\right]^2/4 - 1/\bar{\lambda}_T^{\,2}} & \bar{\lambda}_T \ge 1 \end{cases} \tag{15}$$

where $\varepsilon_1 = 0.499\bar{\lambda}_T$ -0.074; and $\varepsilon_2 = 1.461\bar{\lambda}_T$ -1.036.

EC4 [64] recommends using the buckling curve (a) corresponding to an imperfection factor of 0.21 for the ambient-temperature design of rectangular CFST columns when the reinforcement ratio is less than 3%. For reinforcement ratios between 3% and 6%, the buckling curve (b) corresponding to an imperfection factor of 0.34 should be used. As for the fire limit state design of CFST columns, EC4 [59] recommends that the reduction coefficient of buckling curve (c) corresponding to an imperfection factor of 0.49 should be adopted. However, Leskela [65] and Aribert et al. [66] suggested that the use of EC4 [59] buckling curve (c) should be revised. Wang [67] suggested to use buckling curve (a) for unreinforced CFST columns when using the EC4 high-temperature concrete constitutive model, whereas when Lie's [43] concrete model is used, buckling curve (c) is recommended. Albero et al. [68] proposed a simple calculation model for concrete filled hollow sections exposed to fire all around the column according to the standard temperature-time curve, which has been recently incorporated as a normative method in Annex H of prEN 1994-1-2:2021. This New Annex H

EN 1994-1-2 method suggests to use buckling curve (a) for unreinforced CFST columns and buckling curve (b) for reinforced columns.

For ambient-temperature design, the $\varphi - \bar{\lambda}$ relationships of these four buckling curves are shown in Fig. 20(b). The EC3 buckling curve (a) results in the largest φ, whereas the JGJ/T471 buckling curve leads to the smallest φ.

The applicability of these four buckling curves for the determination of the high-temperature buckling resistance $N_{b,T}$ of square TRC columns are assessed and compared in Fig. 20(c). The mean values of the ratios between the calculated and FEA results are 0.94, 1.05, 1.00 and 0.95, when using the JGJ/T471, EC3 (a), EC3 (b) and EC3 (c) buckling curves, respectively. The corresponding standard deviations are 0.10, 0.09, 0.09 and 0.09.

As mentioned in Section 4.2, the sectional aspect ratio has little influence on the fire resistance of rectangular TRC columns. It is, therefore, speculated that the above-mentioned calculation method for square TRC columns is also applicable to rectangular TRC columns. This speculation is evaluated against FEA results. The variable D in Eq. (10) and Eq. (12) is replaced by D_{eq}. The calculated results are compared to the FEA results in Fig. 20(d). The mean values of the ratios between the calculated and FEA results are 0.94, 1.04, 1.00 and 0.96, when using the JGJ/T471, EC3 (a), EC3 (b) and EC3 (c) buckling curves, respectively. The corresponding standard deviations are 0.09, 0.09, 0.09 and 0.09. Since the design method has been developed for TRC columns with idealized pinned boundary conditions and rotational end restraints exist in the fire tests in this study, it is not possible to validate the design method against the test results.

The applicability of the New Annex H EN 1994-1-2 method to TRC columns was assessed. Figs. 20(e) and 20(f) compare the calculated buckling resistance $N_{b,T}$ with FEA results. The average ratios between the calculated and FEA results of square and rectangular TRC columns are 1.02 and 1.00, respectively. The corresponding standard deviations are 0.18 and 0.22, which are considerably higher than the standard deviations resulted from the method presented in this paper. The inherent difference between the TRC and CFST columns may be the reason behind the relatively high result deviations of the New Annex H EN 1994-1-2 method. The design method proposed in this paper is developed to be consistent with the

ambient-temperature design method of TRC columns given in Chinese code [15] and also to cover protected columns.

For both square and rectangular TRC columns, the EC3 buckling curve (a) leads to the most unsafe prediction, and the JGJ/T471 buckling curve results in the most conservative prediction. The EC3 (c) buckling curve seems to offer the most optimum solution in terms of both safety and efficiency. However, as the JGJ/T471 and EC3 (c) buckling curves lead to very similar results, these two buckling curves are recommended for the calculation of the high-temperature buckling resistance of square and rectangular TRC columns.

5.3 Protected TRC columns

Fire protection may be needed for TRC columns with small dimensions, large slendernesses or high load ratios. Sprayed cementitious coating is a commonly-used fire protection for steel and composite members in China. The influence of fire protection thickness on the fire resistance of TRC columns was analysed using the heat transfer and stress analysis models built in Section 2 and the results for square TRC columns and rectangular TRC columns are shown in Fig. 21 and Fig. 22, respectively. In the heat transfer model, the inner surface of the fire protection is tied to the outer surface of the steel tube. The thermal properties of the fire protection are assumed to remain constant during heating. The thermal properties of cementitious fire protection recommended by GB 50936 [60] are adopted, which are thermal conductivity = 0.116 W/(m·°C), specific heat = 1024 J/(kg·°C) and density = 400 kg/m^3. The fire protection is modelled using the DC3D8 element of ABAQUS, with the same mesh as for the steel tube. At least four elements are assigned throughout the thickness of the fire protection. As shown in Figs. 21 and 22, the column fire resistance increases almost linearly with the increase of the protection thickness and the influence of sectional aspect ratio on the fire resistance of protected rectangular TRC columns is very slight.

To consider the influence of the thermal protection on the steel tube temperature, Eq. (3) was modified as Eq. (16). An equivalent heating time t_{es} is introduced, which is the time at which the steel tube temperature of an unprotected column is the same as that of a protected column at an arbitrary heating time t (as in Eq. (3)). A similar correction method is also used in GB

50936 [60] for the determination of the steel tube temperature of protected CFST columns.

$$T_s = 1080 - 450\exp(-0.8t_{es}) - 630\exp(-3t_{es}) + 20 \quad (16)$$

where $t_{es} = t/(\frac{1}{m_s}\frac{d_p}{k_p} + 1)$; d_p (in mm) is the protection thickness; k_p (in W/(m·°C)) is the protection conductivity; m_s is a coefficient derived from regression analysis and $m_s = 1.73/D_{eq} + 6.51$, where D_{eq} (in m) is the equivalent sectional dimension; for square columns, $D_{eq} = D$; for rectangular columns, $D_{eq} = (D \cdot B)^{1/2}$. The value of m_s decreases with an increase of D_{eq}, reflecting that fire protection measures are more effective for columns of larger dimensions than those of smaller section sizes.

Eq. (16) was validated against heat transfer FEA modelling. For the square columns of 200 mm width, the influence of the conductivity k_p (0.08, 0.107, 0.116, 0.151, 0.171, 0.191 W/(m·°C)) of the fire protection material was investigated when the coating thickness d_p was 15 mm. When the conductivity was fixed to 0.116 W/(m·°C), columns with different protection thicknesses (5, 10, 15, 20, 25 and 30 mm) were studied. Figs. 23(a) and 23(b) compare the steel tube temperature-time curves predicted by FEA and those calculated using Eq. (16). The results calculated using the GB 50936 [60] equations for CFST columns were also included in these figures for comparison purposes. Both Eq. (16) and the GB 50936 [60] equations compare well with the FEA results. The rebar temperatures were calculated using Eq. (16) and Eq. (4), and compared with the FEA results in Figs. 23(c)-23(f). A good agreement was also achieved.

Eq. (16) was further validated for square and rectangular columns of larger dimensions (400-1500 mm) and of different protection thicknesses (2-20 mm) and the results are shown in Fig. 24. The protection conductivity is assumed to be 0.116 W/(m·°C) for all cases. As presented in Figs. 24(a)-24(d), Eq. (16) still gives good predictions for steel tube temperatures in square sections, compared with FEA results. However, the GB 50936 equations overestimate the steel tube temperatures and the overestimation increases with an increase of the section size. This might be because that the coefficient m_s given in GB 50936 is a constant, which does not vary with the variations of sectional dimensions. For rectangular TRC columns with different aspect ratios, the steel tube temperatures predicted by Eq. (16) were also validated well

against the FEA results, as shown in Figs. 24(e)-24(h).

As for the concrete core in protected TRC columns, the equivalent strength reduction factor k_{cfT} and equivalent stiffness reduction factor k_{cET} were obtained from FEA modelling. Figs. 25(a)-25(d) illustrate the relationships between the equivalent strength reduction factor and heating time for square columns of different dimensions and different protection thicknesses. The fire protection significantly delays the decrease of the equivalent strength of concrete during heating, compared to unprotected cases. For square columns with $D \geqslant 600$ mm and of $d_p \geqslant 5$ mm, the strength reduction is very limited, i.e. k_{cfT} remains larger than 0.9, up to 4 hours' heating. The development of the stiffness reduction during heating for square columns is shown in Figs. 25(e)-25(h). Same as the cases of unprotected columns, the equivalent stiffness of protected columns is also found to decrease faster than the equivalent strength as temperature rises. Fig. 26 plots the equivalent reduction factors of the concrete core in protected rectangular TRC columns and the influence of section aspect ratio is found to be insignificant.

In order to consider the influence of fire protection on the equivalent reduction factors of the concrete core, Eq. (6) and Eq. (9) were modified into Eq. (17) and Eq. (18), respectively. The two coefficient m_{cf} and m_{cE} were determined by regression analysis.

$$k_{cfT} = 1 - (\frac{0.045}{D_c} - 0.016)t_{ecf} \tag{17}$$

$$T_{cE,eq} = \frac{-9.8t_{ecE}{}^2 + 92.7t_{ecE}}{D_c} + 20 \tag{18}$$

where $t_{ecf} = t / (\frac{1}{m_{cf}} \frac{d_p}{k_p} + 1)$; $m_{cf} = 40$; $t_{ecE} = t / (\frac{1}{m_{cE}} \frac{d_p}{k_p} + 1)$; $m_{cE} = 40D_{eq} + 46$; D_{eq} (in m) is the equivalent sectional dimension.

The calculated values of k_{cfT} and k_{cET} for protected square and rectangular TRC columns were compared with those from FEA, as shown in Figs. 27(a) and 27(b).

The correction coefficient β in Section 5.2 was also modified as,

$$\beta = \frac{1}{1 + (0.0054t_{e\beta} + 0.22)\sqrt{\frac{t_{e\beta}}{D_c}}} \tag{19}$$

where $t_{e\beta} = t / (\frac{1}{m_\beta} \frac{d_p}{k_p} + 1)$; m_β =40.

To sum up, the design equations for unprotected square and rectangular TRC columns proposed in Sections 5.1 and 5.2 have been modified into Eqs. (16)-(19) to consider the effect of fire protection for the design of protected square and rectangular TRC columns. The EC3 buckling curve (c) and the JGJ/T471 buckling curve, as recommended in Section 5.2 for unprotected columns were also assessed for their applicability for protected columns. Fig. 27(c) illustrates the comparison between the calculated buckling resistance and the FEA results. Good agreements were achieved, confirming that these two buckling curves can be used for protected square and rectangular TRC columns.

6. Conclusions

A structural fire safety design method for square and rectangular TRC columns is developed in this paper based on fire resistance tests and numerical studies. The following conclusions may be drawn from the results of this research:

- The failure mode of the tested rectangular TRC columns in fire is global buckling resulting runaway horizonal deflection. The temperature gradient along the major axis of a rectangular TRC section is larger than that along the minor axis. A nonlinear 3-D FEA model has been developed and is capable of simulating the fire performance of square and rectangular TRC columns after being validated against the fire test results;
- The fire resistance of square and rectangular TRC columns decreases significantly with an increase of load ratio or slenderness ratio, and larger sectional dimensions lead to higher fire resistance. The influence of sectional aspect ratio on the column fire resistance is marginal. The use of fire protection could enhance the column fire resistance effectively;
- The heat transfer equations given in the Japanese AIJ recommendation [61] are modified to calculate the temperatures of the steel tube and reinforcement bars in square and rectangular TRC sections with or without fire protection. Equations have also been proposed to determine the equivalent temperatures of the concrete core;

- With the consideration of material degradations and thermal stresses, a design method has been proposed to determine the fire resistance of square and rectangular TRC columns with or without fire protection, based on the ambient temperature design method given in the Chinese standard JGJ/T471 [15]. The EC3 [63] buckling curve (c) and the JGJ/T471 buckling curve are recommended to determine the buckling resistance reduction coefficient.

Acknowledgements

The research work in this paper is financially supported by the National Key Research and Development Program (2016YFC0701203) and the National Natural Science Foundation of China (51878220), to which the authors are grateful.

Reference

[1] M. Tomii, K. Sakino, K. Watanabe, Y. Xiao, Lateral load capacity of reinforced concrete short columns confined by steel tube, Proceedings of the International Speciality Conference on Concrete Filled Steel Tubular Structures, Harbin, China (1985), 19-26

[2] M. Tomii, K. Sakino, Y. Xiao, K, Watanabe, Earthquake resisting hysteretic behavior of reinforced concrete short columns confined by steel tube, Proceedings of the International Speciality Conference on Concrete Filled Steel Tubular Structures, Harbin, China (1985), 119-125

[3] R.S. Aboutaha, R.I. Machado, Seismic resistance of steel-tubed high-strength reinforced-concrete columns, J. Struct. Eng. 125 (1999) 485-494.

[4] K. Lahlou, M. Lachemi, P.C. AÏtcin, Confined high-strength concrete under dynamic compressive loading, J. Struct. Eng. 125 (1999) 1100-1108.

[5] Y.P. Sun, K. Sakino, Earthquake-resisting performance of RC columns confined by square steel tube, Part 3: effects of shear span ratio of column, J. Struct. Constr. Eng. AIJ. 547 (2001) 129-136.

[6] L.H. Han, H. Qu, Z. Tao, Z.F. Wang, Experimental behaviour of thin-walled steel tube confined concrete column to RC beam joints under cyclic loading, Thin-Walled Struct. 47

(2009) 847–857.

[7] S.M. Zhang, J.P. Liu, Seismic behavior and strength of square tube confined reinforced-concrete (STRC) columns, J. Constr. Steel Res. 63 (2007) 1194-1207.

[8] J.P. Liu, S.M. Zhang, X.D. Zhang, L.H. Guo, Behavior and strength of circular tube confined reinforced-concrete (CTRC) columns, J. Constr. Steel Res. 65 (2009) 1447-1458.

[9] X.D. Wang, J.P. Liu, S.M. Zhang, Behavior of short circular tubed-reinforced-concrete columns subjected to eccentric compression, Eng. Struct. 105 (2015) 77-86.

[10] X.H. Zhou, J.P. Liu, X.D. Wang, Y.F. Chen, Behavior and design of slender circular tubed-reinforced-concrete columns subjected to eccentric compression, Eng. Struct. 124 (2016) 17-28.

[11] L.H. Guo, Y. Liu, F. Fu, H.J. Huang, Behavior of axially loaded circular stainless steel tube confined concrete stub columns, Thin-Walled Struct. 139(6) (2019) 66-76.

[12] Y.Y. Wang, L.G. Yang, H. Yang, C.Y. Liu, Behaviour of concrete-filled corrugated steel tubes under axial compression, Eng. Struct. 183 (2019) 475-495.

[13] L.G. Yang, Y.Y. Wang, M. Elchalakani, Y. Fang, Experimental behavior of concrete-filled corrugated steel tubular short columns under eccentric compression and non-uniform confinement, Eng. Struct. 2020, 220.

[14] Zhou XH, Liu JP. Performance and design of steel tube confined concrete members. Beijing China: Science Press Ltd.; 2010 [in Chinese].

[15] JGJ/T471, Technical Standard for Steel Tube Confined Concrete Structures, MOHURD (Ministry of Housing and Urban-Rural Development of the People's Republic of China), Beijing, China, 2020 [In Chinese]

[16] L.H. Han. Concrete Filled Steel Tubular Structures-Theory and Practice (third edition), Science Press, Beijing (China) (2016) [in Chinese]

[17] T.T. Lie, V.K.R. Kodur, Fire resistance of steel columns filled with bar-reinforced concrete, J. Struct. Eng. 122 (1996) 30-36.

[18] Y.C. Wang, Steel and composite structures, behaviour and design for fire safety, Spon Press, London (2002)

[19] V.K.R. Kodur, Performance-based fire resistance design of concrete-filled steel columns,

J. Constr. Steel Res. 51 (1999) 21-36.

[20] M.L. Romero, V. Moliner, A. Espinos, C. Ibañez, A. Hospitaler, Fire behavior of axially loaded slender high strength concrete-filled tubular columns, J. Constr. Steel Res. 67 (2011) 1953-1965.

[21] Z. Tao, M. Ghannam, T.Y. Song, L.H. Han, Experimental and numerical investigation of concrete-filled stainless steel columns exposed to fire, J. Constr. Steel Res. 118 (2016) 120-134.

[22] H. Yang, L.H. Han, Y.C. Wang, Effects of heating and loading histories on post-fire cooling behaviour of concrete-filled steel tubular columns, J. Constr. Steel Res. 64 (2008) 556-570.

[23] M. Pagoulatou, T. Sheehan, X.H. Dai, D. Lam, Finite element analysis on the capacity of circular concrete-filled double-skin steel tubular (CFDST) stub columns, Eng. Struct. 72 (2014) 102–112.

[24] F.Q. Liu, Y.Y. Wang, L. Gardner, A.H. Varma, Experimental and numerical studies of reinforced concrete columns confined by circular steel tubes exposed to fire, J. Struct. Eng. 145 (2019) 04019130.

[25] D.D. Yang, F.Q. Liu, S.S. Huang, H. Yang, ISO 834 standard fire test and mechanism analysis of square tubed-reinforced-concrete columns, J. Constr. Steel Res. 175 (2020), 106316.

[26] ISO 834-1, Fire Resistance Test–Elements of Building Construction, Part 1: General Requirements, International Organization for Standardization ISO 834, Geneva, Switzerland, 1999.

[27] EN 1991-1-2, Eurocode 1 - Actions on Structures - Part 1–2: General Actions - Actions on Structures Exposed to Fire, CEN, Brussels, 2002.

[28] ECCS, Fire Safety of Steel Structures: Technical Note, Calculation of the Fire Resistance of Centrally Loaded Composite Steel-Concrete Columns Exposed to the Standard Fire vol. 3, European Convention for Constructional Steelwork Technical Committee, Brussels, Belgium, 1988.

[29] H. Yang, F.Q. Liu, L. Gardner, Performance of concrete-filled RHS columns exposed to

fire on 3 sides, Eng. Struc. 56 (2013) 1986-2004.

[30] H. Yang, F.Q. Liu, L. Gardner, Post-fire behaviour of slender reinforced concrete columns confined by circular steel tubes, Thin-Walled Struct. 87 (2015) 12-29.

[31] F.Q. Liu, H. Yang, L. Gardner, Post-fire behaviour of eccentrically loaded reinforced concrete columns confined by circular tubes, J. Constr. Steel Res. 122 (2016) 495-510.

[32] F.Q. Liu, H. Yang, R. Yan, W. Wang, Experimental and numerical study on behaviour of square steel tube confined reinforced concrete stub columns after fire exposure, Thin-Walled Struct. 139 (2019) 105-125.

[33] F.Q. Liu, H. Yang, W. Wang, Behaviours of concentrically and eccentrically loaded square steel tube confined reinforced concrete slender columns after fire exposure, Thin-Walled Struct. 158 (2021) 107155

[34] L.H. Han, W.H. Wang, H.X. Yu, Analytical behaviour of RC beam to CFST column frames subjected to fire, Eng. Struct. 36 (2012) 394-410.

[35] L.H. Han, K. Zhou, Q.H. Tan, T.Y. Song, Performance of steel-reinforced concrete column after exposure to fire: FEA model and experiments, J. Struct. Eng. 142 (2016) 04016055.

[36] L.H. Han, T.Y. Song, K. Zhou, Z.Q. Cui, Fire performance of CFST triple-limb laced columns, J. Struct. Eng. 144 (2018) 04018157.

[37] T.Y. Song, L.H. Han, H.X. Yu, Temperature field analysis of SRC-column to SRC-beam joints subjected to simulated fire including cooling phase, Adv. Struct. Eng. 14 (2011) 353-366.

[38] J. Ding, Y.C. Wang, Realistic modelling of thermal and structural behaviour of unprotected concrete filled tubular columns in fire, J. Constr. Steel Res. 64 (2008) 1086-1102.

[39] Y.F. Yang, F. Fu, Fire resistance of steel beam to square CFST column composite joints using RC slabs: Experiments and numerical studies, Fire Safety J. 104 (2019) 90-108.

[40] L. Xu, Y.B. Liu, Concrete filled steel tube reinforced concrete (CFSTRC) columns subjected to ISO-834 standard fire: experiment, Adv. Struct. Eng. 16 (2013) 1263-1282.

[41] CIDECT, Improvement and extension of the simple calculation method for fire

resistance of unprotected concrete filled hollow columns, Final Report, CIDECT Research Project 15Q, 2004.

[42] X.T. Lv, H. Yang, S.M. Zhang, Effect of contact thermal resistance on temperature distributions of concrete-filled steel tubes in fire, J Harbin Inst Technol. 18 (2011) 81-88.

[43] T.T. Lie, Fire resistance of circular steel columns filled with bar-reinforced concrete, J. Struct. Eng. 120 (1994) 1489-1509.

[44] S. Hong, A.H. Varma, Analytical modeling of the standard fire behavior of loaded CFT columns, J. Constr. Steel Res. 65 (2009) 54-69.

[45] J.S. Huo, G.W. Huang, Y. Xiao, Effects of sustained axial load and cooling phase on post-fire behaviour of concrete-filled steel tubular stub columns, J. Constr. Steel Res. 65 (2009) 1664-1676.

[46] Q.H. Tan, L.H. Han, H.X. Yu, Fire performance of concrete filled steel tubular (CFST) column to RC beam joints, Fire Safety J. 51 (2012) 68-84.

[47] EN 1992-1-2, Eurocode 2 - Design of Concrete Structures - Part 1-2: General Rules - Structural Fire Design, CEN, Brussels, 2004.

[48] EN 1993-1-2, Eurocode 3 - Design of Steel Structures - Part 1-2: General Rules - Structural Fire Design, CEN, Brussels, 2005.

[49] ISO 12570, Hygrothermal Performance of Building Materials and Products-Determination of Moisture Content by Drying at Elevated Temperature, International Organization for Standardization ISO 12570, Geneva, Switzerland, 2000.

[50] A. Espinos, M.L. Romero, E. Serra, A. Hospitaler, Experimental investigation on the fire behaviour of rectangular and elliptical slender concrete-filled tubular columns, Thin-Walled Struct. 93 (2015) 137-148.

[51] M. Neuenschwander, M. Knobloch, M. Fontana, Modeling thermo-mechanical behavior of concrete-filled steel tube columns with solid steel core subjected to fire, Eng. Struct. 136 (2017) 180-193.

[52] Lie TT, Chabot M. Experimental studies on the fire resistance of hollow steel columns filled with plain concrete. Ottawa, Canada: NRC-CNRC, Inst. Res. Constr., Internal Rep. No. 611; 1992.

[53] Chabot M, Lie TT. Experimental studies on the fire resistance of hollow steel columns filled with bar-reinforced concrete. Ottawa, Canada: NRC-CNRC, Inst. Res. Constr., Internal Rep. No. 628; 1992.

[54] L.H. Han, Y.F. Yang, L. Xu, An experimental study and calculation on the fire resistance of concrete-filled SHS and RHS columns, J. Constr. Steel Res. 59 (2003) 427-52.

[55] A. Espinos, M.L. Romero, E. Serra, A. Hospitaler, Circular and square slender concrete-filled tubular columns under large eccentricities and fire, J. Constr. Steel Res. 110 (2015) 90-100.

[56] A. Espinos, M.L. Romero, A. Hospitaler, Advanced model for predicting the fire response of concrete filled tubular columns, J. Constr. Steel Res. 66 (2010) 1030–1046.

[57] Lie T T, Woollerton J L. Fire Resistance of Reinforced Concrete Columns. Ottawa, Canada: NRC-CNRC, Inst. Res. Constr., Internal Rep. No. 569; 1988.

[58] Hass R. Practical Rules for the Design of Reinforced Concrete and Composite Columns Submitted to Fire. German: T.U. Braunschweig, Technical Rep. No. 69; 1986.

[59] EN 1994-1-2, Eurocode 4 - Design of Composite Steel and Concrete Structures - Part 1–2: General Rules - Structural Fire Design, CEN, Brussels, 2008.

[60] GB 50936, Technical Code for Concrete Filled Steel Tubular Structures, MOHURD (Ministry of Housing and Urban-Rural Development of the People's Republic of China), Beijing, China, 2014 [In Chinese]

[61] AIJ, Recommendations for Design and Construction of Concrete-Filled Steel Tubular Structures, Architectural Institute of Japan, Tokyo, Japan, 2008 [In Japanese]

[62] D.D. Yang, F.Q. Liu, H. Yang, Comparison on fire performance of circular and square steel tube confined reinforced concrete columns, J. Build. Struct. 39 (2018) 65-73. [in Chinese]

[63] EN 1993-1-1, Eurocode 3 - Design of Steel Structures - Part 1-1: General Rules and Rules for Buildings, CEN, Brussels, 2005.

[64] EN 1994-1-1, Eurocode 4 - Design of Composite Steel and Concrete Structures - Part 1-1: General Rules and Rules for Buildings, CEN, Brussels, 2004.

[65] Leskela MV. Inconsistencies in the fire design rules of composite columns to EN 1994-

1-2. Steel Concrete Composite and Hybrid Structures, Leeds, England; 2009: 489–494.

[66] Aribert JM, Renaud C, Zhao B. Simplified fire design for composite hollow-section columns, Struct. Build. 161 (2008) 325-336.

[67] Wang YC. Some considerations in the design of unprotected concrete-filled steel tubular columns under fire conditions. J Construct Steel Res. 1997; 44(3): 203–23.

[68] V. Albero, A. Espinos, M.L. Romero, A. Hospitaler, G. Bihina, C. Renaud, Proposal of a new method in EN1994-1-2 for the fire design of concrete-filled steel tubular columns, Eng. Struct. 128 (2016) 237-255.

Notation

t_{FR}	fire resistance
n	load ratio
N_f	applied constant axial load in fire
N_b	ambient-temperature buckling resistance
$N_{u,T}$	high-temperature compressive resistance
$N_{b,T}$	high-temperature buckling resistance
$N_{cr,T}$	Euler buckling load at high temperature
φ	ambient-temperature buckling reduction coefficient
φ_T	high-temperature buckling reduction coefficient
D	depth of the rectangular section or dimension of the square section
B	width of the rectangular section
D_{eq}	equivalent sectional dimension of the rectangular section
D_c	equivalent sectional dimension of the inner concrete core
x	the larger one of the distances from the temperature calculated node to the section's symmetric axes
y	the smaller one of the distances from the temperature calculated node to the section's symmetric axes
D_1	sectional dimension of the concrete core corresponding to x
D_2	sectional dimension of the concrete core corresponding to y
L	whole column length
L_e	exposed column length
L_{eff}	effective column length
d	distance from a temperature measuring point to the perimeter of the concrete core
k	sectional aspect ratio
λ	slenderness ratio
λ_D	slenderness ratio for major axis buckling
λ_B	slenderness ratio for minor axis buckling
$\bar{\lambda}$	ambient-temperature relative slenderness
$\bar{\lambda}_T$	high-temperature relative slenderness
t_s	thickness of the steel tube
ϕ	diameter of the reinforcing bar
d_p	thickness of the fire protection
k_p	conductivity of the fire protection
α_s	steel ratio
ρ	longitudinal reinforcement ratio
A_s	sectional area of the steel tube
A_c	sectional area of the concrete
A_b	sectional area of the reinforcing bars
I_s	moment of inertia of the steel tube
I_c	moment of inertia of the concrete core
I_b	moment of inertia of the reinforcing bars
f_y	ambient-temperature yield strength of the steel tube
f_{cu}	ambient-temperature concrete cube compressive strength
f_c'	ambient-temperature concrete cylinder compressive strength
f_{cc}	compressive strength of confined concrete at ambient temperature
f_b	ambient-temperature yield strength of the reinforcing bar
$f_{y,T}$	high-temperature yield strength of the steel tube
$f_{c,T}'$	high-temperature concrete cylinder compressive strength
$f_{c,eq,T}$	equivalent compressive strength of the unconfined concrete at high temperature

$f_{cc,T}$	compressive strength of confined concrete at high temperature
$f_{b,T}$	high-temperature yield strength of the rebar
E_s	ambient-temperature elastic modulus of the steel tube
E_c	ambient-temperature elastic modulus of the concrete
E_b	ambient-temperature elastic modulus of the reinforcing bar
$E_{c,eq,T}$	equivalent elastic modulus of the concrete core at high temperature
$(EI)_{fi,eff}$	effective flexural stiffness of the column in fire
k_{cfT}	equivalent strength reduction factor of the concrete core
k_{cET}	equivalent stiffness reduction factor of the concrete core
k_{yT}	high-temperature strength reduction factor of the structural steel
k_{bT}	high-temperature strength reduction factor of the reinforcing bar
k_{sET}	high-temperature elastic modulus reduction factor of the structural steel
k_{bET}	high-temperature elastic modulus reduction factor of the reinforcing bar
t	heating time
T	temperature
T_s	temperature of the steel tube
T_b	temperature of the reinforcing bar
$T_{cf,eq}$	equivalent strength temperature of the concrete core
$T_{cE,eq}$	equivalent stiffness temperature of the concrete core

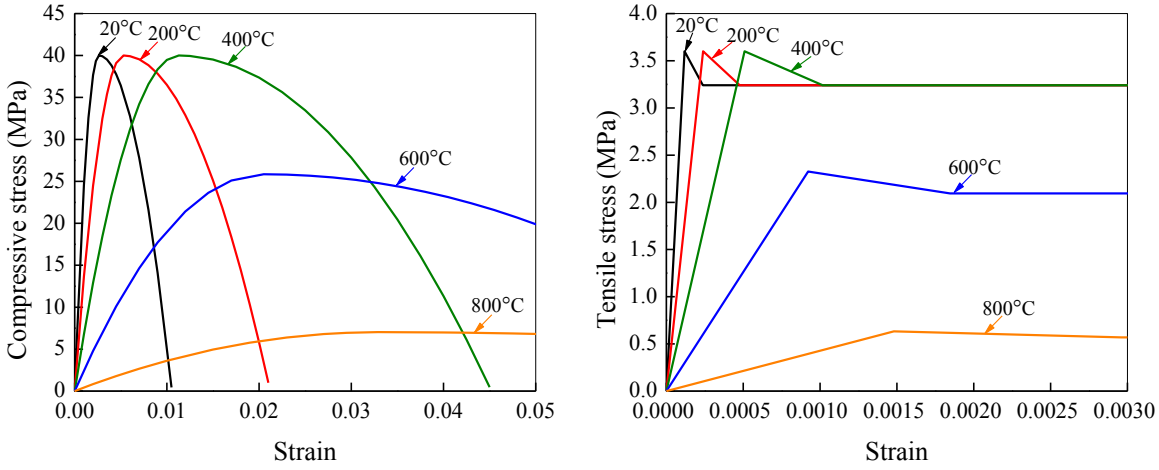

(a) Compressive curves (b) Tensile curves

Fig. 1. Stress-strain curves at different temperatures for concrete of cylinder compressive strength 40 MPa

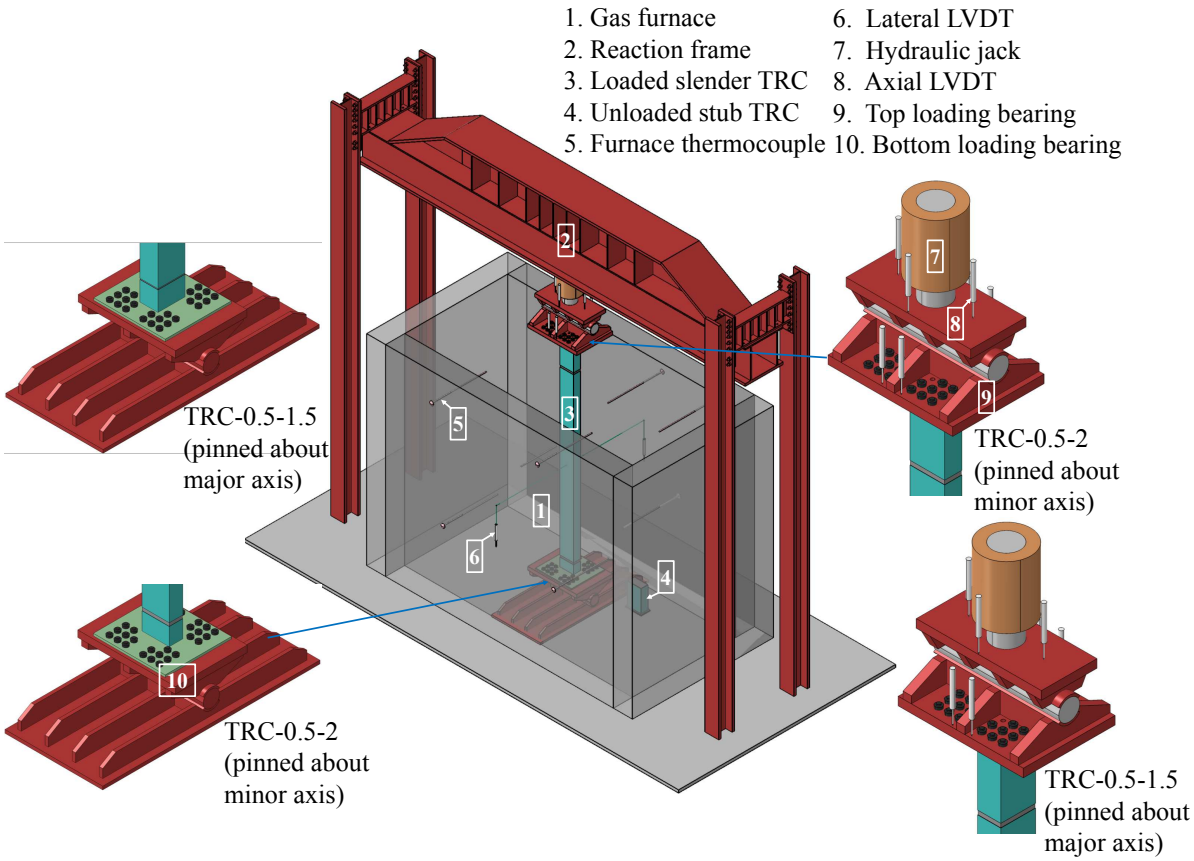

(a) Schematic view

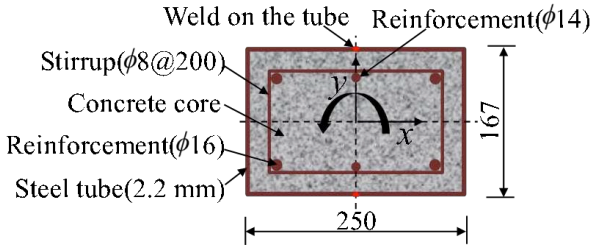

(b) Cross-section details (TRC-0.5-1.5)

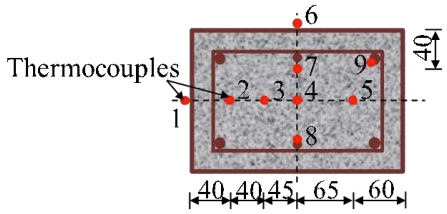

(c) Thermocouples (TRC-0.5-1.5)

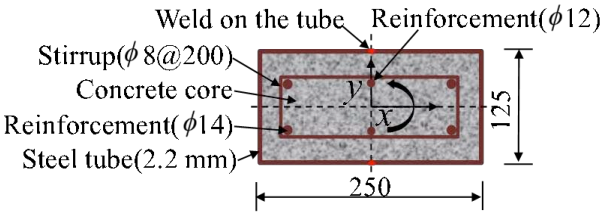

(d) Cross-section details (TRC-0.5-2)

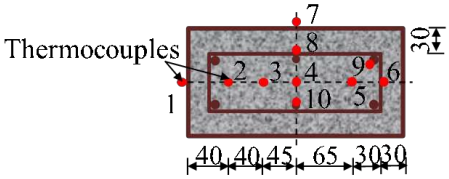

(e) Thermocouples (TRC-0.5-2)

Fig. 2. Schematic view, cross-section details and thermocouple locations of the rectangular TRC specimens (unit: mm)

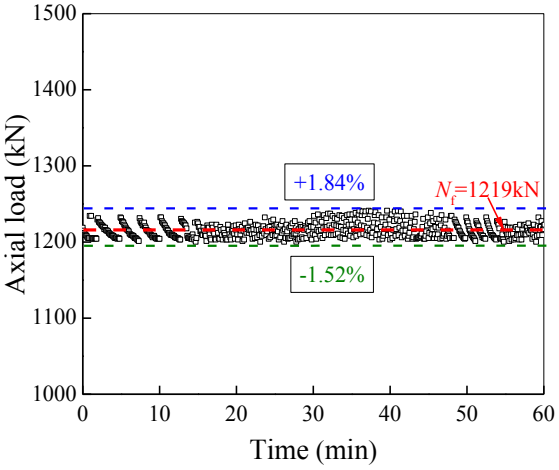

(a) Loading history (TRC-0.5-1.5)

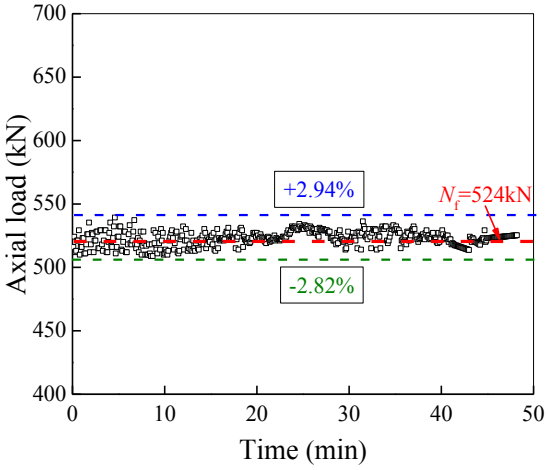

(b) Loading history (TRC-0.5-2)

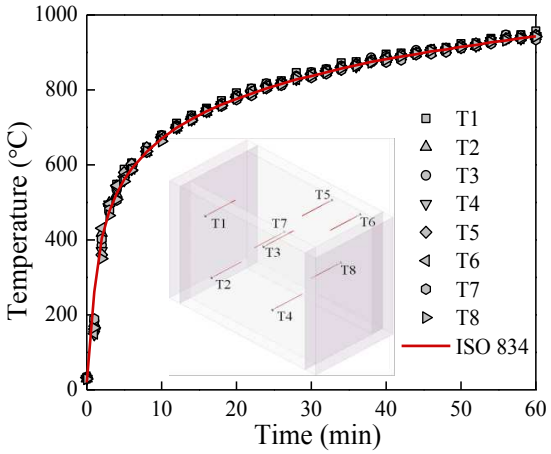

(c) Furnace temperatures (TRC-0.5-1.5)

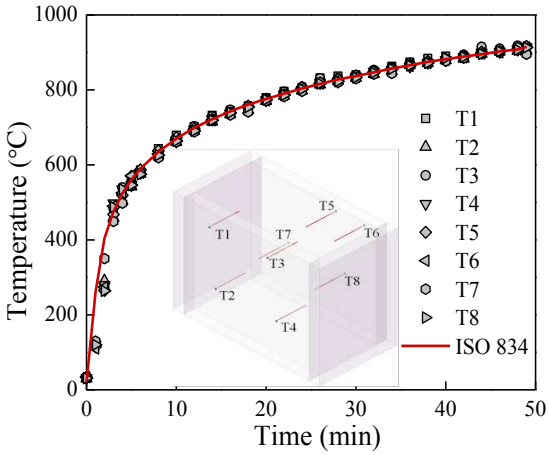

(d) Furnace temperatures (TRC-0.5-2)

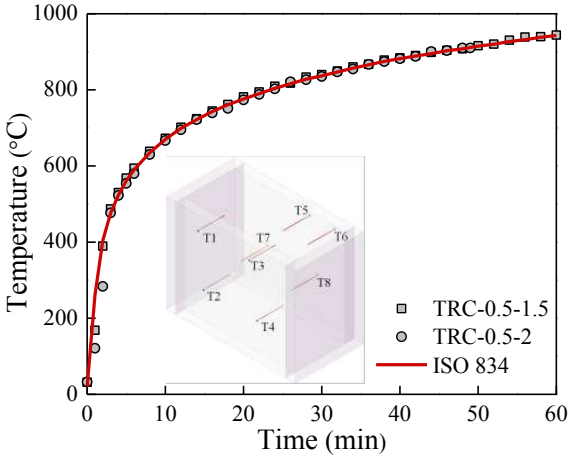

(e) Average furnace temperatures

Fig. 3. Loading and heating control in the fire tests

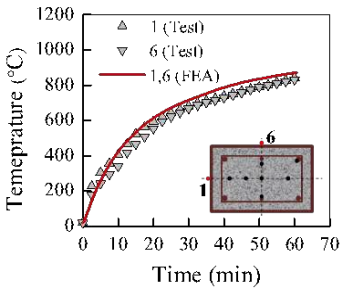

(a) Points 1, 6 (TRC-0.5-1.5)

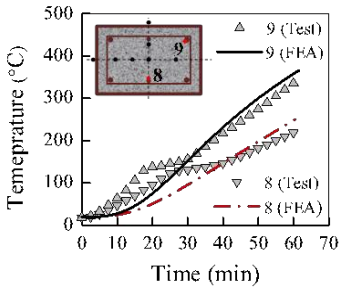

(b) Points 8, 9 (TRC-0.5-1.5)

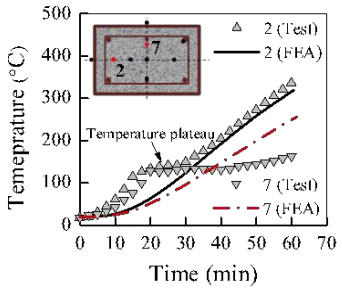

(c) Points 2, 7 (TRC-0.5-1.5)

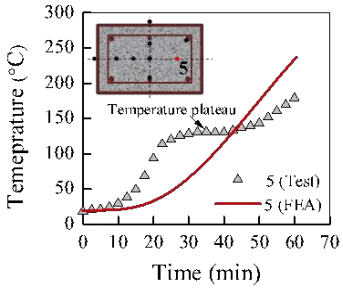

(d) Point 5 (TRC-0.5-1.5)

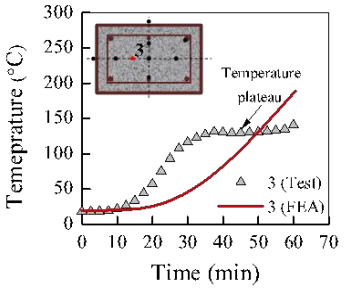

(e) Point 3 (TRC-0.5-1.5)

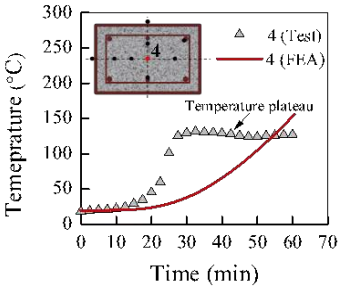

(f) Point 4 (TRC-0.5-1.5)

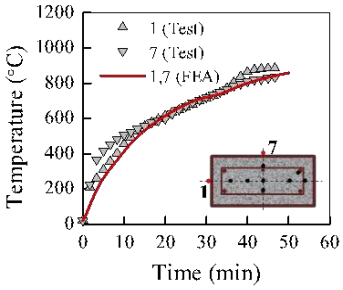

(g) Points 1, 7 (TRC-0.5-2)

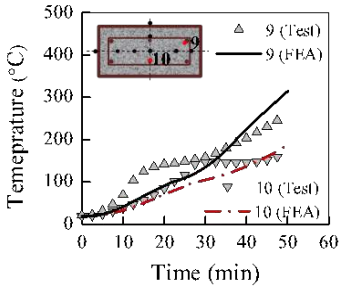

(h) Points 9, 10 (TRC-0.5-2)

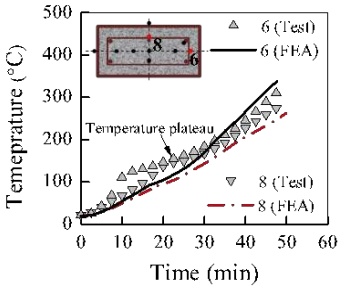

(i) Points 6, 8 (TRC-0.5-2)

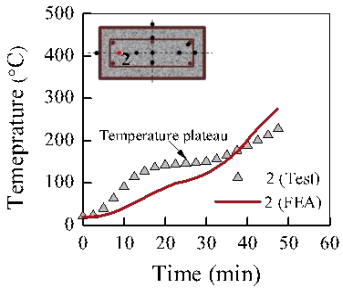

(j) Point 2 (TRC-0.5-2)

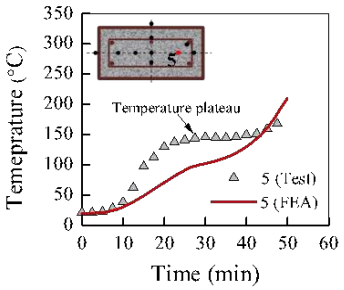

(k) Point 5 (TRC-0.5-2)

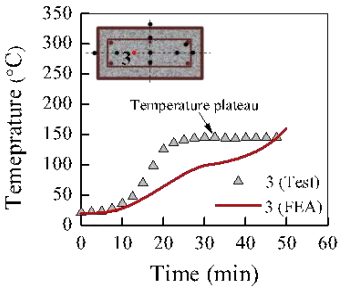

(l) Point 3 (TRC-0.5-2)

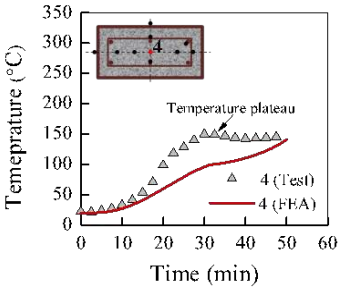

(m) Point 4 (TRC-0.5-2)

Fig. 4. Temperature-time curves of the tested rectangular TRC columns

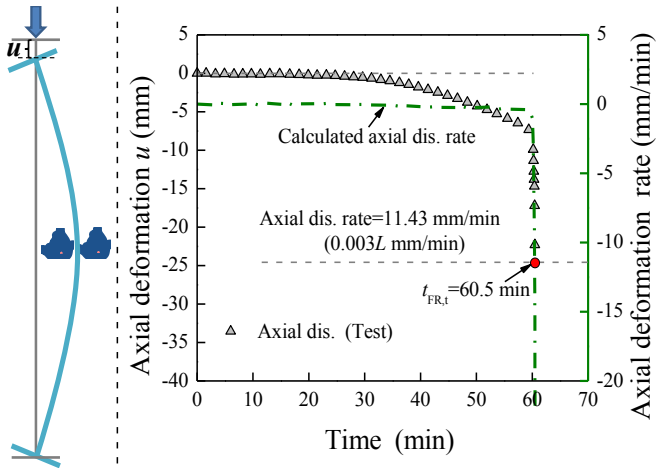

(a) Measured axial deformation (TRC-0.5-1.5)

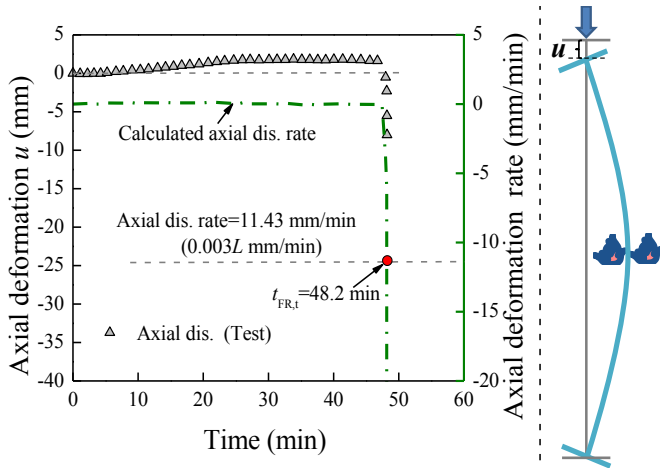

(b) Measured axial deformation (TRC-0.5-2)

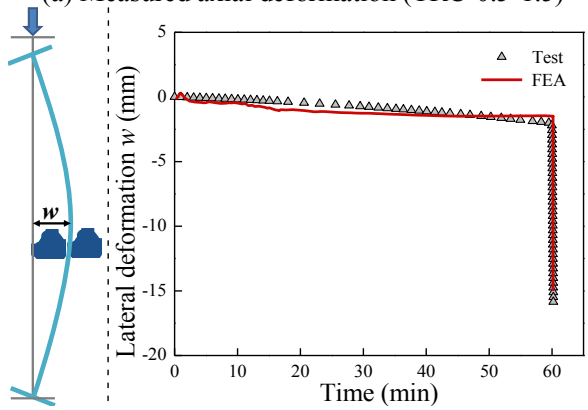

(c) Lateral deformation (TRC-0.5-1.5)

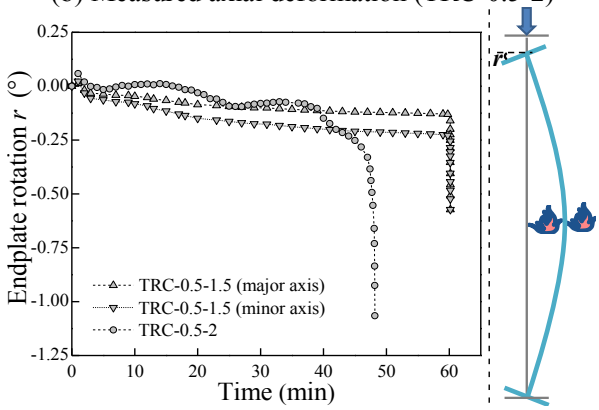

(d) Endplate rotation

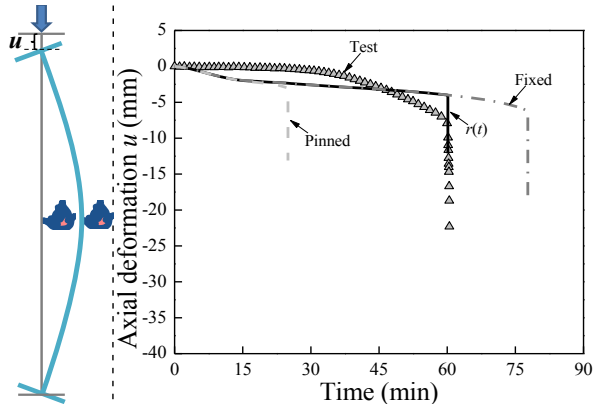

(e) Predicted axial deformation (TRC-0.5-1.5)

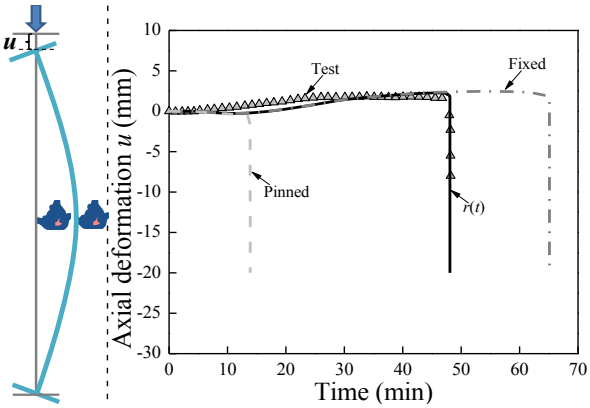

(f) Predicted axial deformation (TRC-0.5-2)

Fig. 5. Measured and predicted deformation-time curves of the tested rectangular TRC specimens

(a) TRC-0.5-1.5 (major axis bending)

(b) TRC-0.5-1.5 (minor axis bending)

(c) TRC-0.5-2

Fig. 6. Failure modes of the tested rectangular TRC columns after fire tests

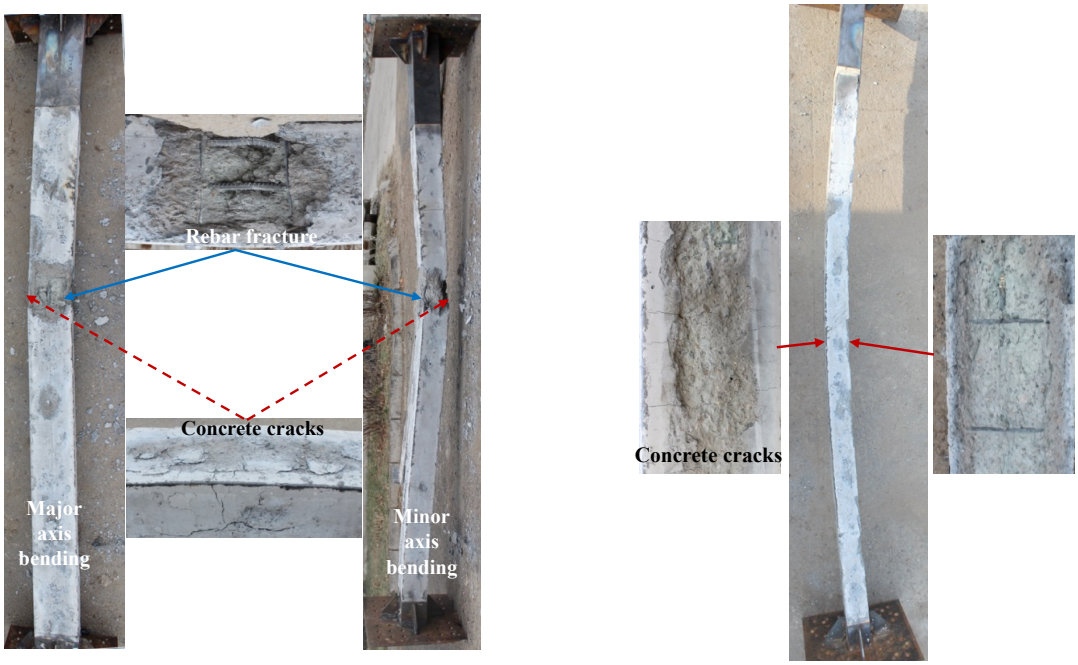

(a) TRC-0.5-1.5 (b) TRC-0.5-2

Fig. 7. Concrete cores and rebars of the tested rectangular TRC specimens after fire tests

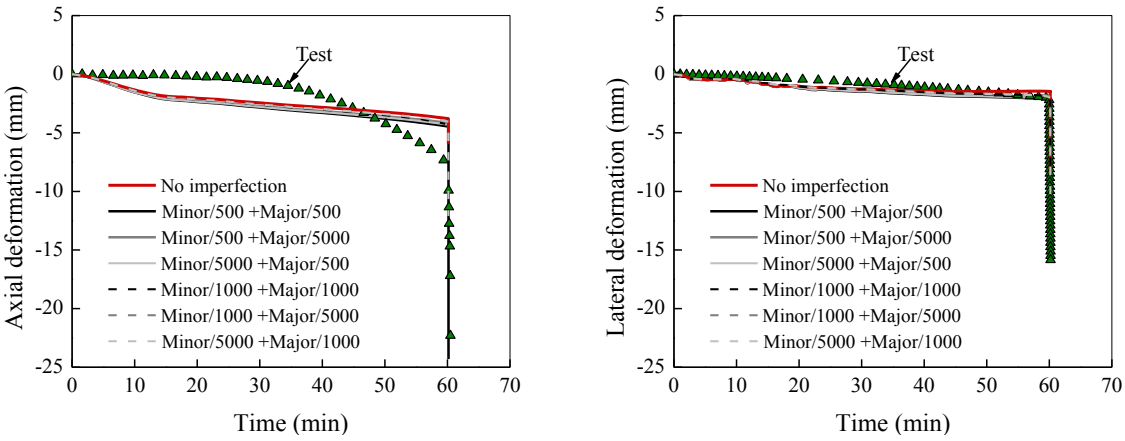

(a) Axial deformation (b) Lateral deformation

Fig. 8. Influence of global imperfections on the predicted deformation-time curves of TRC-0.5-1.5

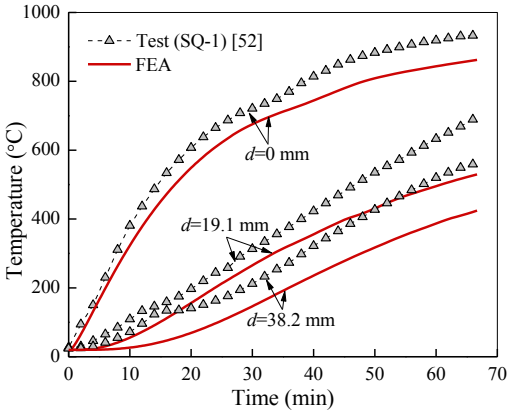

(a) SQ-1

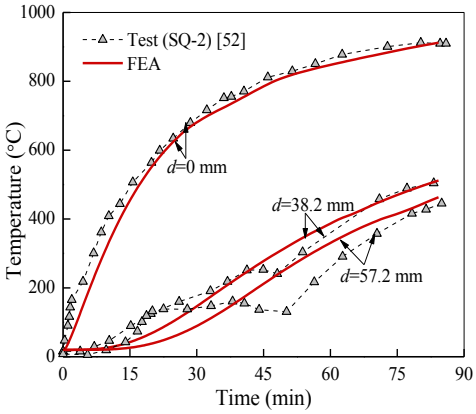

(b) SQ-2

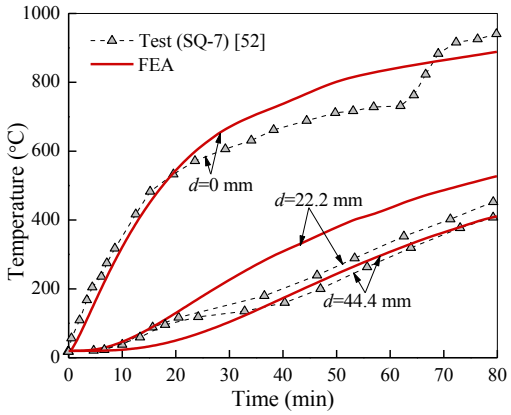

(c) SQ-7

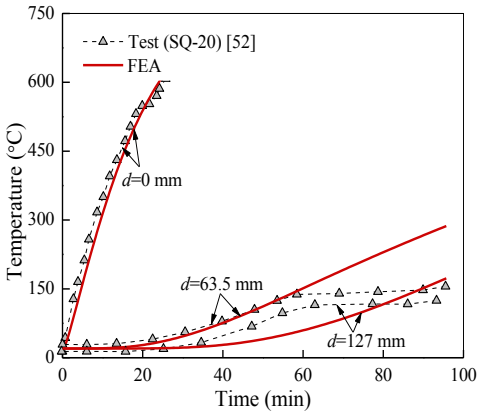

(d) SQ-20

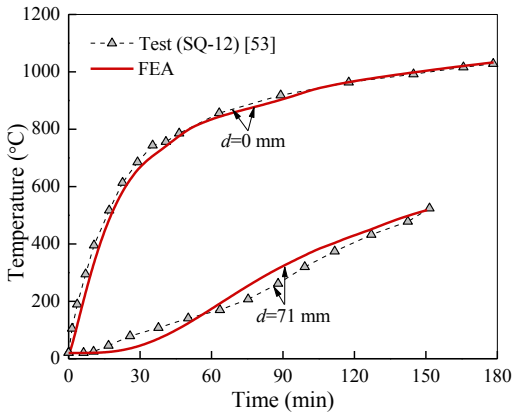

(e) SQ-12

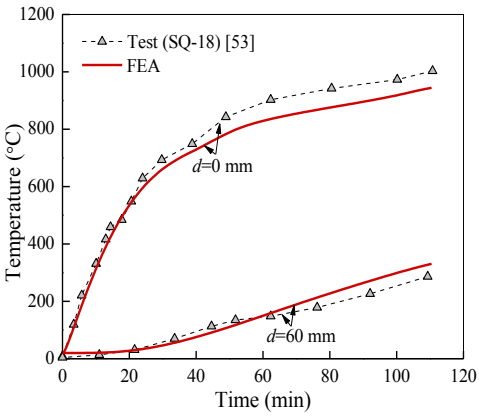

(f) SQ-18

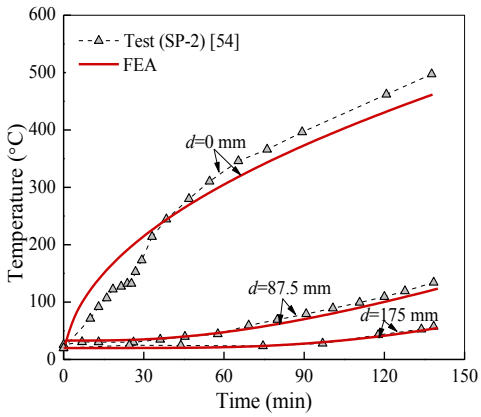

(g) SP-2

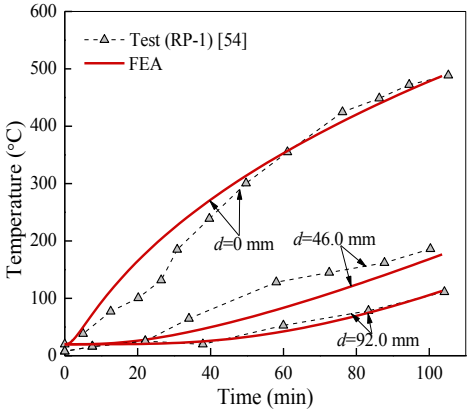

(h) RP-1

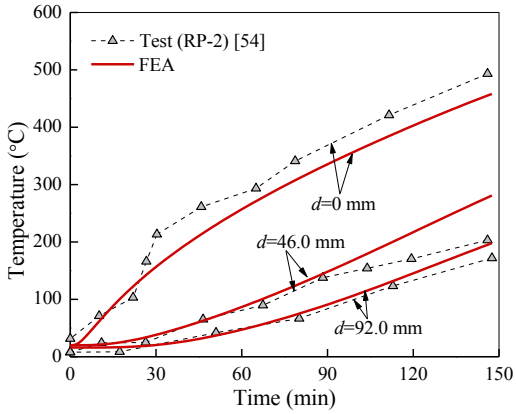

(i) RP-2

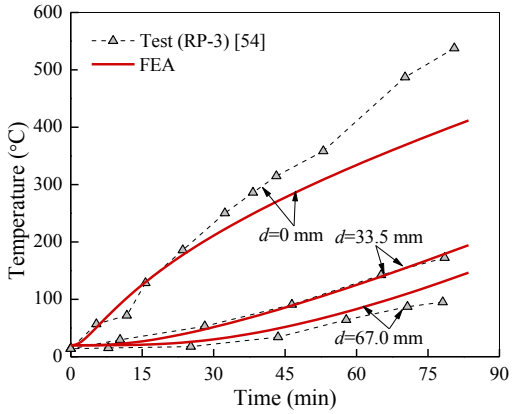

(j) RP-3

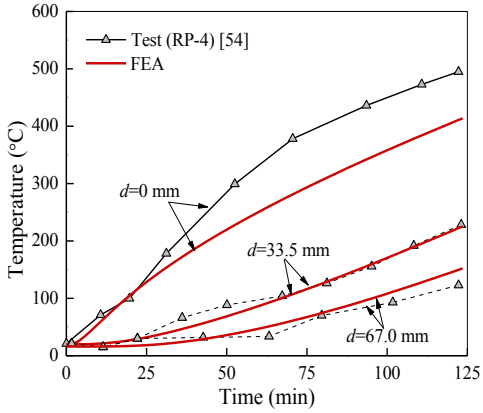

(k) RP-4

Fig. 9. Comparisons of temperature-time curves between FEA and experiments on CFST columns conducted by other researchers

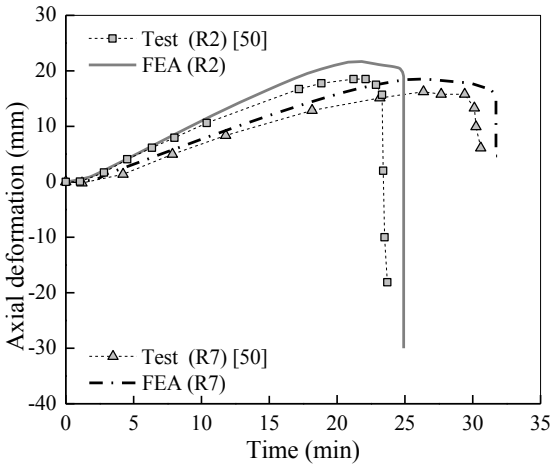

(a) R2 and R7

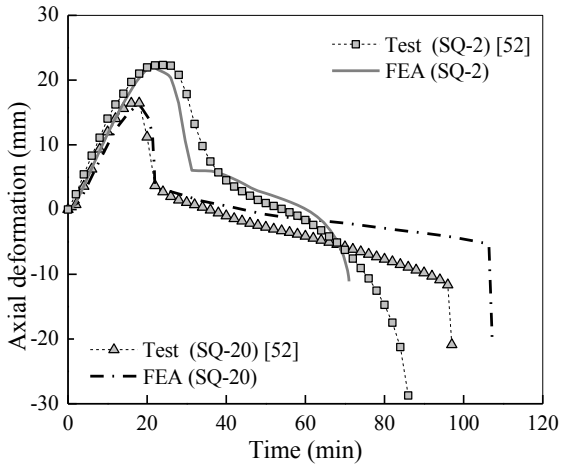

(b) SQ-2 and SQ-20

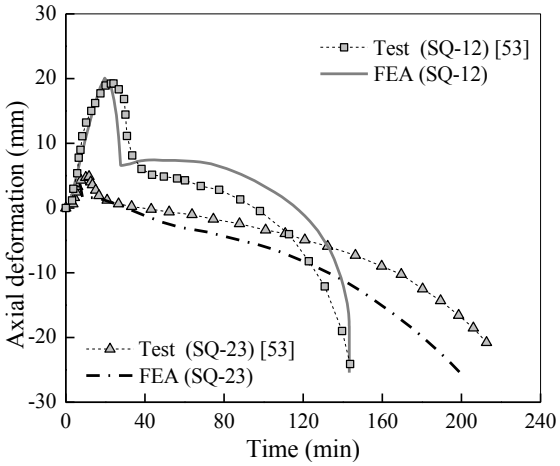

(c) SQ-12 and SQ-23

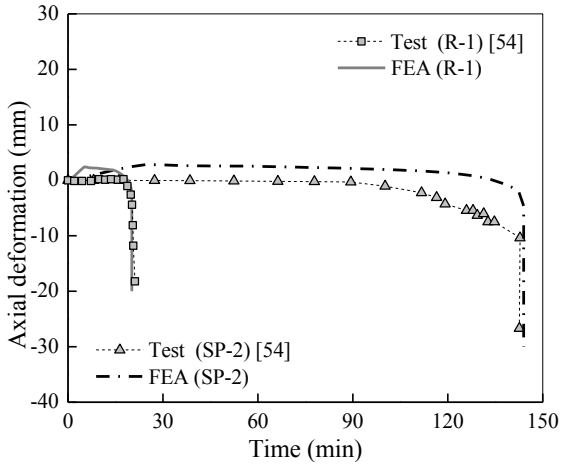

(d) R-1 and SP-2

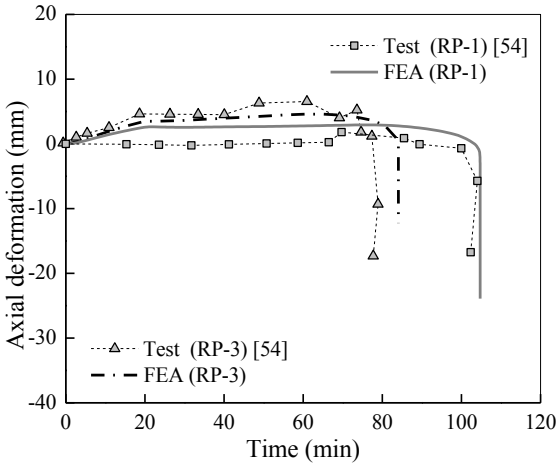

(e) RP-1 and RP-3

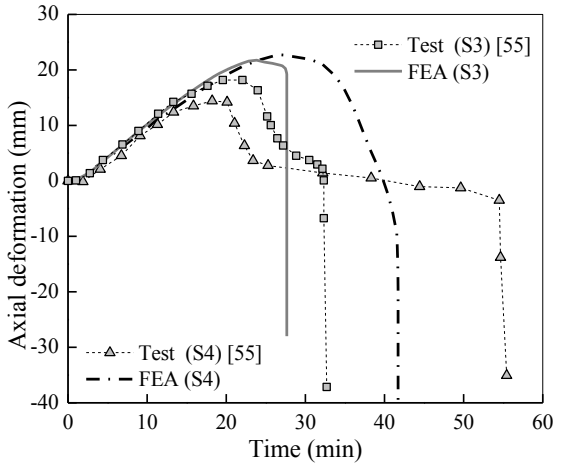

(f) S3 and S4

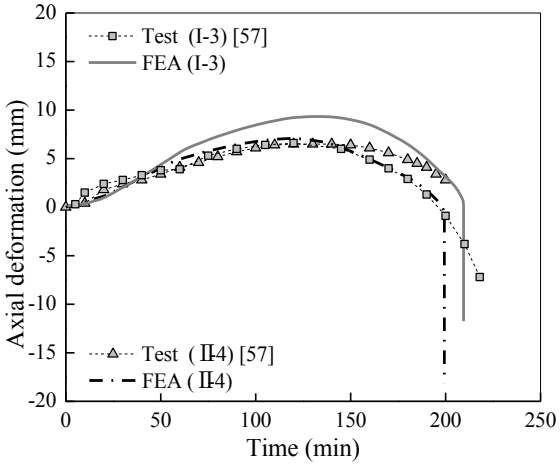

(g) Ⅰ-3 and Ⅱ-4

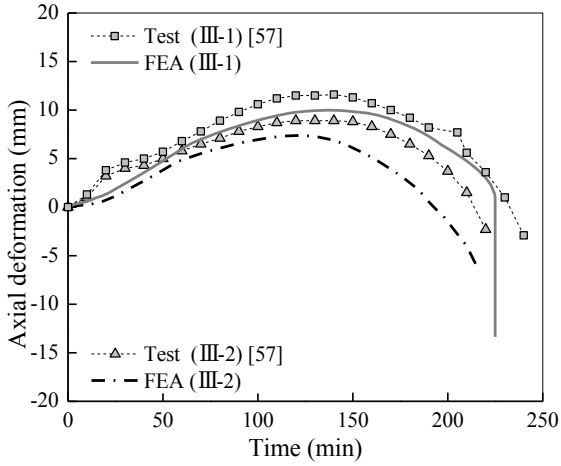

(h) Ⅲ-1 and Ⅲ-2

Fig. 10. Axial deformation-time curves given by FEA vs other researchers' test results on CFST and RC columns

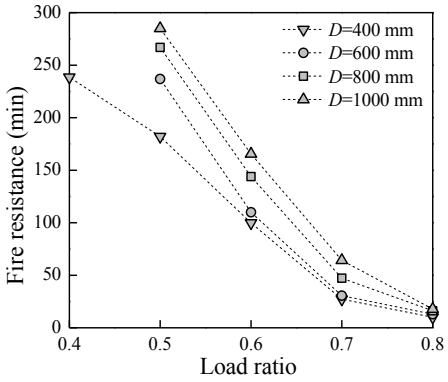

(a) Load ratio

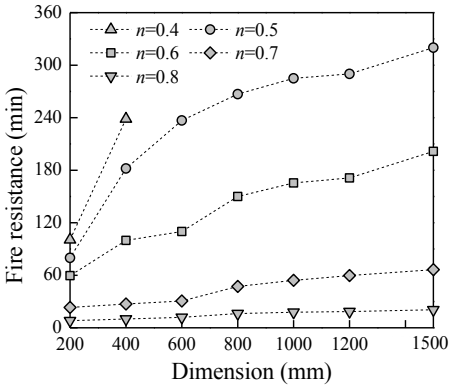

(b) Dimension

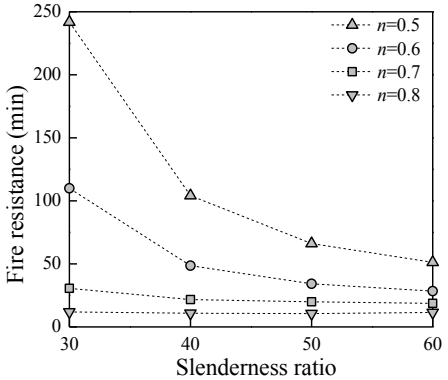

(c) Slenderness ratio

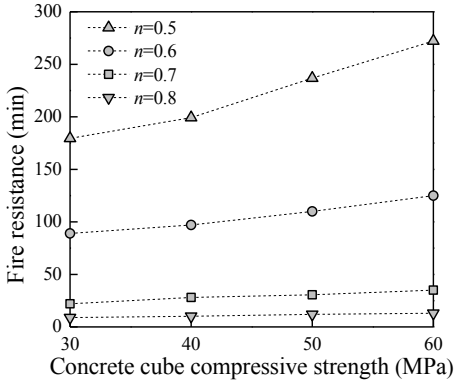

(d) Concrete cube compressive strength

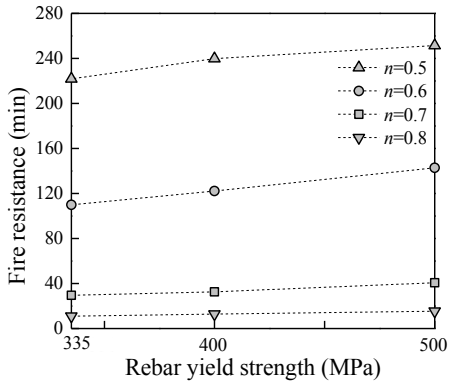

(e) Rebar yield strength

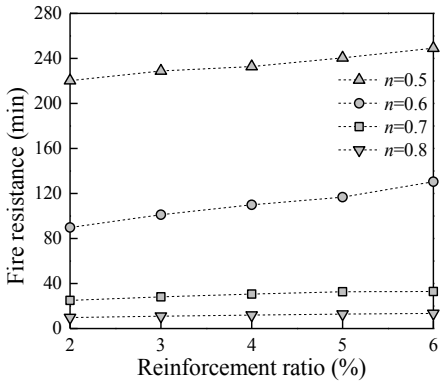

(f) Reinforcement ratio

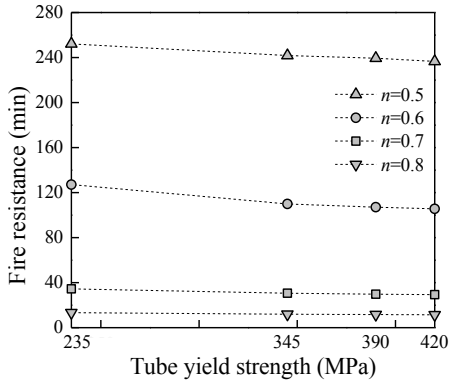

(g) Tube yield strength

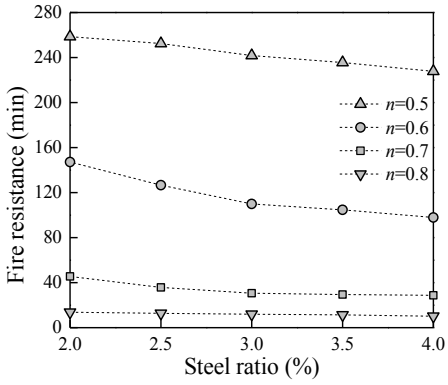

(h) Steel ratio

Fig. 11. Influence of investigated parameters on the fire resistance of square TRC columns

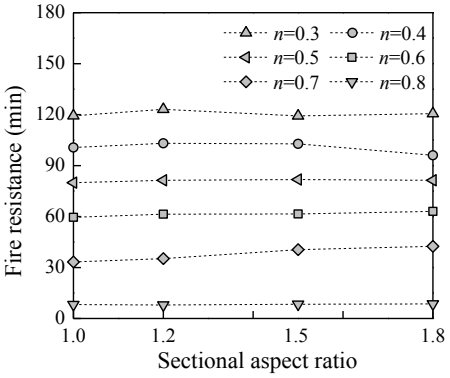

(a) D_{eq}=200 mm

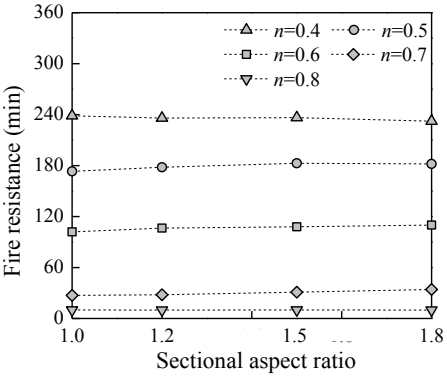

(b) D_{eq}=400 mm

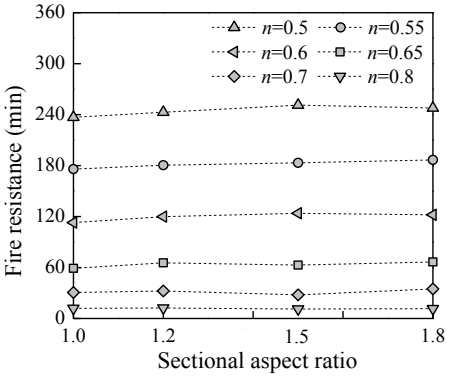

(c) D_{eq}=600 mm

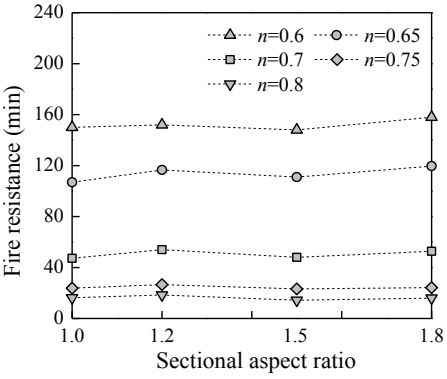

(d) D_{eq}=800 mm

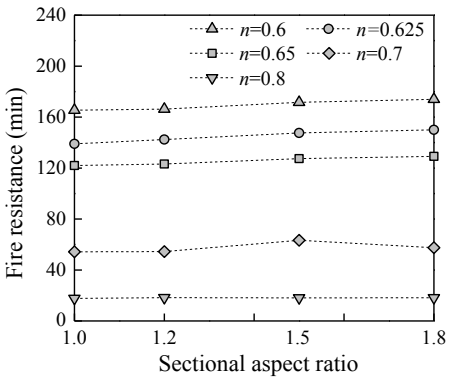

(e) D_{eq}=1000 mm

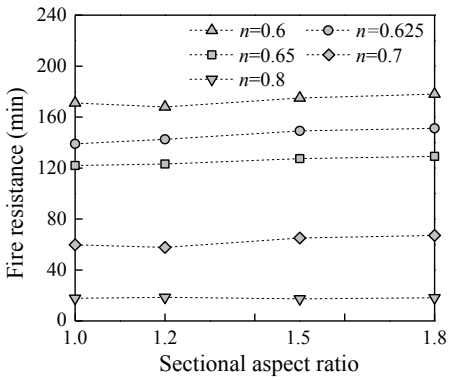

(f) D_{eq}=1200 mm

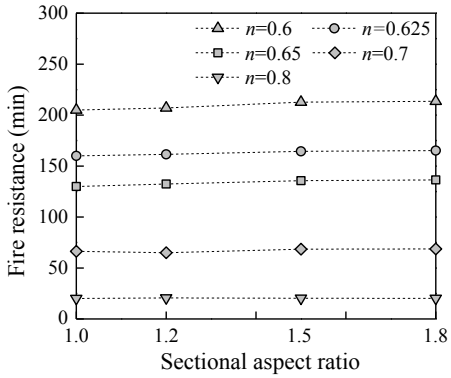

(g) D_{eq}=1500 mm

Fig. 12. Influence of sectional aspect ratio on the fire resistance of rectangular TRC columns

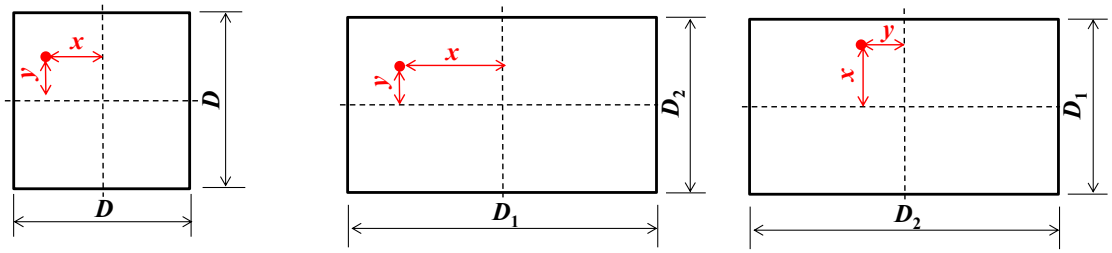

(a) Square section (b) Rectangular section- Ⅰ (c) Rectangular section- Ⅱ

Fig. 13. Illustrations of the rebar locations in the temperature calculations

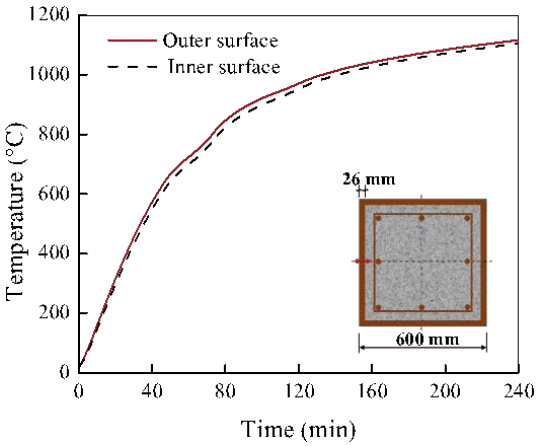

Fig. 14. Temperature difference between the inner and outer surface of a CFST column (D=600 mm, t_s=26 mm)

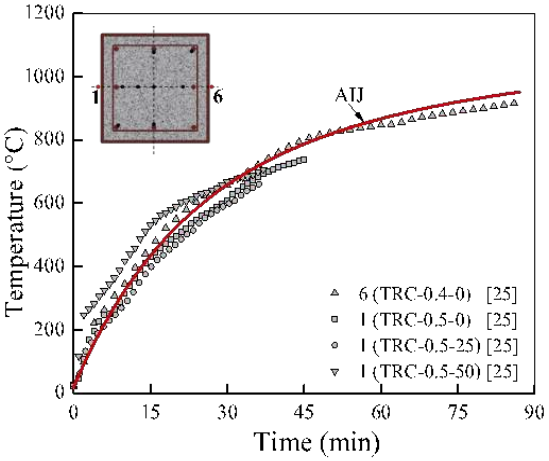

(a) AIJ vs Test (steel tube)

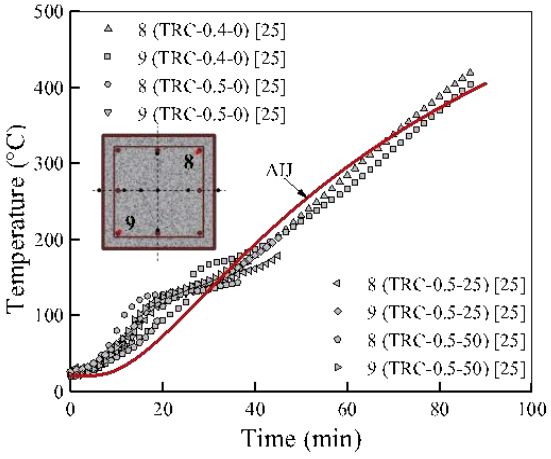

(b) AIJ vs Test (corner rebars)

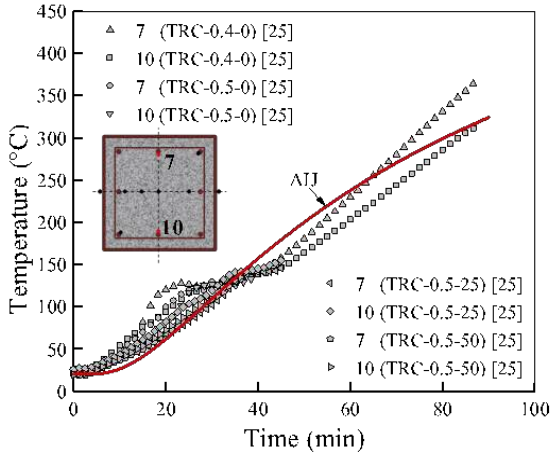

(c) AIJ vs Test (middle rebars)

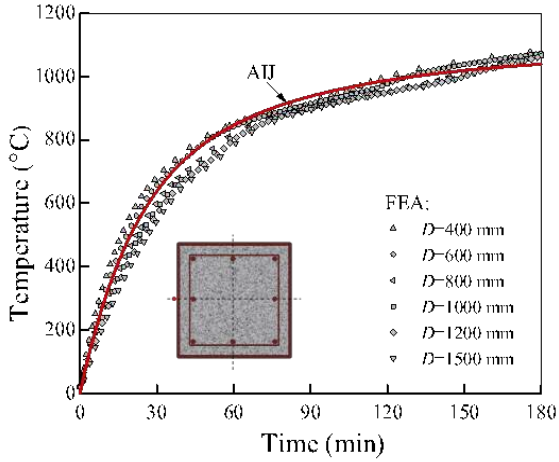

(d) AIJ vs FEA (steel tube)

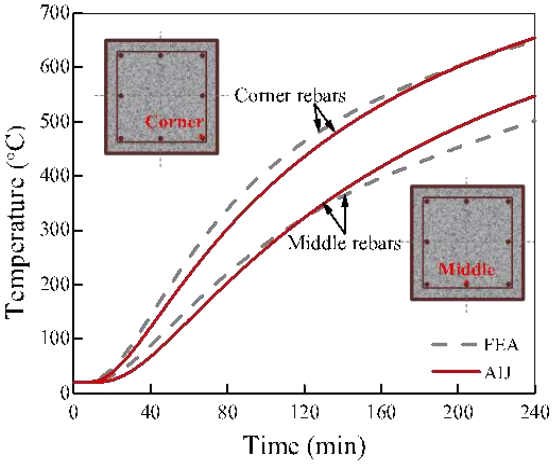

(e) AIJ vs FEA (rebars, *D*=400 mm)

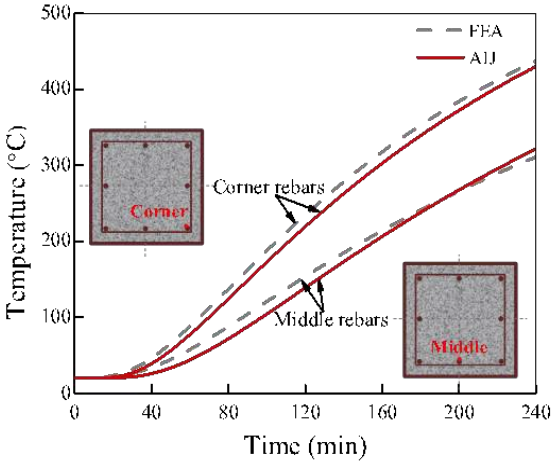

(f) AIJ vs FEA (rebars, *D*=1000 mm)

Fig. 15. Comparisons of temperature results of steel tube and rebars between AIJ and test & FEA results for square TRC columns

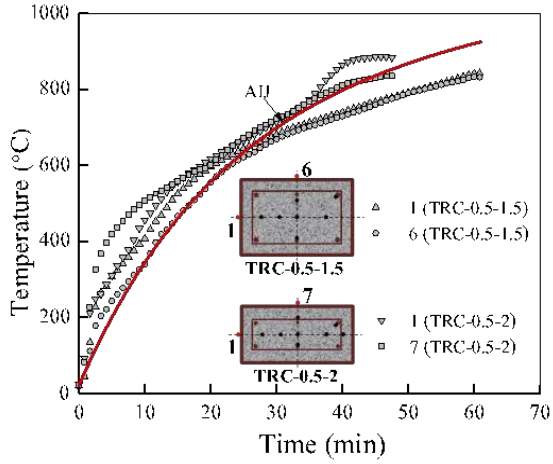

(a) AIJ vs Test (steel tube)

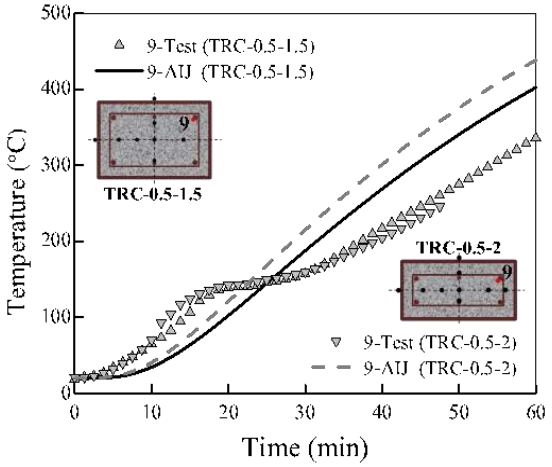

(b) AIJ vs Test (corner rebars)

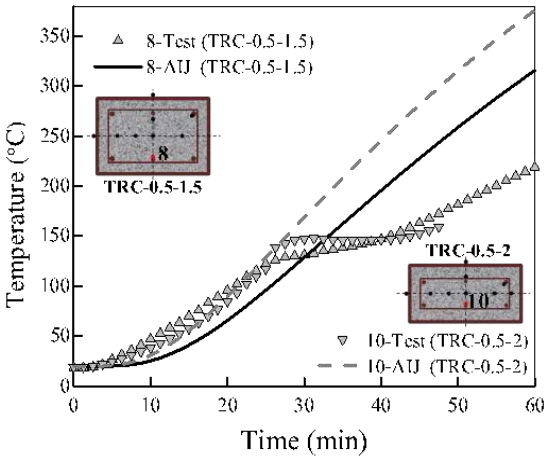

(c) AIJ vs Test (middle rebars)

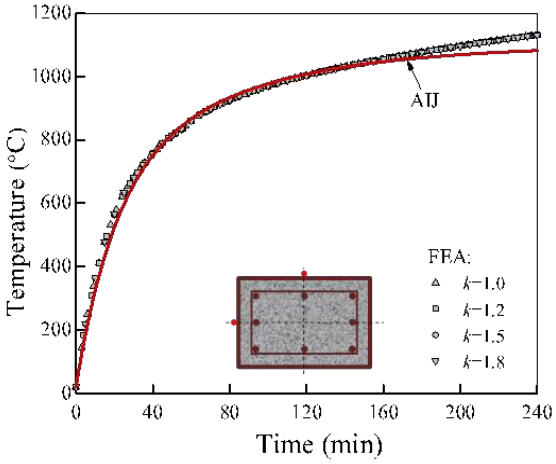

(d) AIJ vs FEA (steel tube, D_{eq}=400 mm)

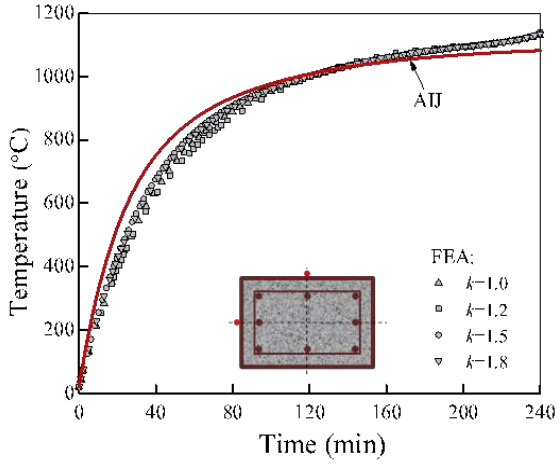

(e) AIJ vs FEA (steel tube, D_{eq}=1000 mm)

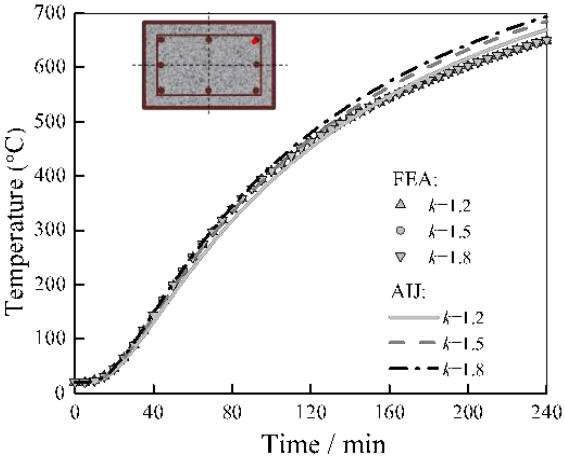

(f) AIJ vs FEA (corner rebars, D_{eq}=400 mm)

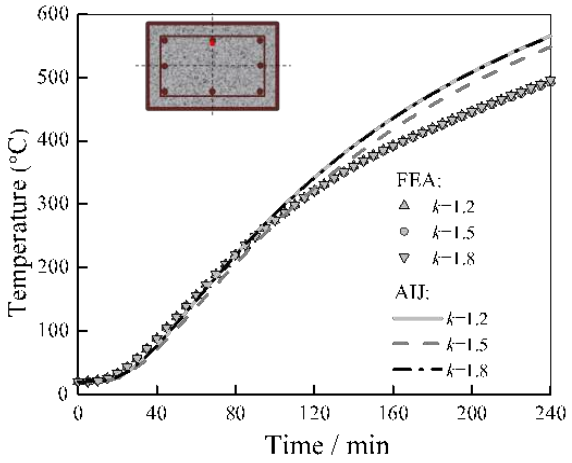

(g) AIJ vs FEA (depth middle rebars, D_{eq}=400 mm)

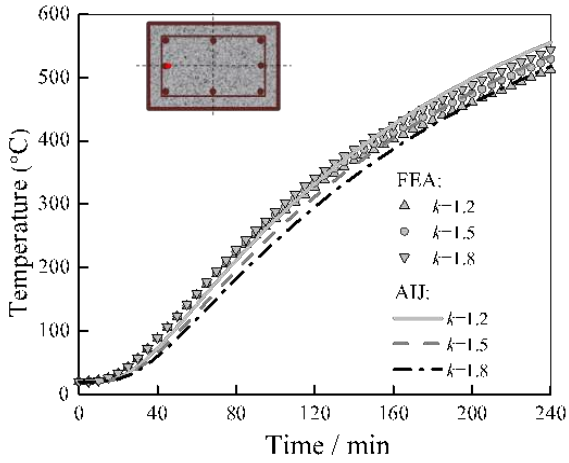

(h) AIJ vs FEA (width middle rebars, D_{eq}=400 mm)

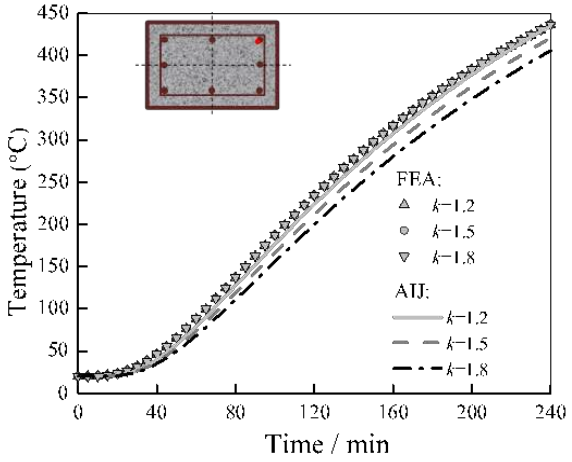

(i) AIJ vs FEA (corner rebars, D_{eq}=1000 mm)

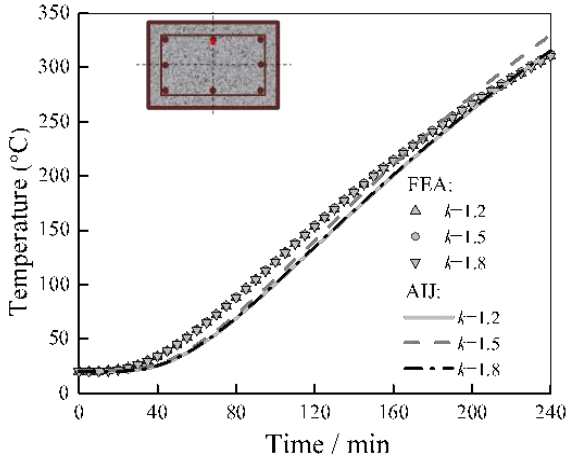

(j) AIJ vs FEA (depth middle rebars, D_{eq}=1000 mm)

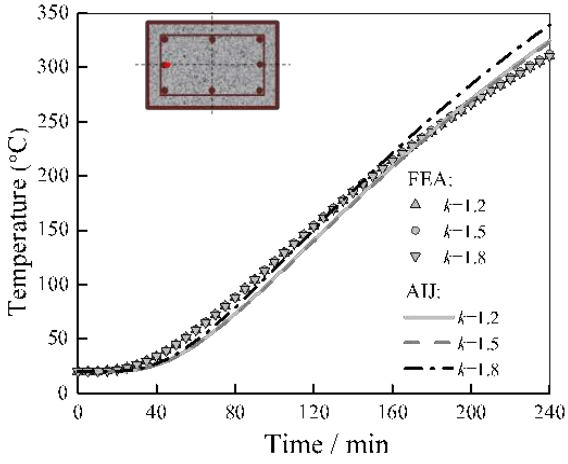

(k) AIJ vs FEA (width middle rebars, D_{eq}=1000 mm)

Fig. 16. Comparisons of temperature results of steel tube and rebars between AIJ and test & FEA results for rectangular TRC columns

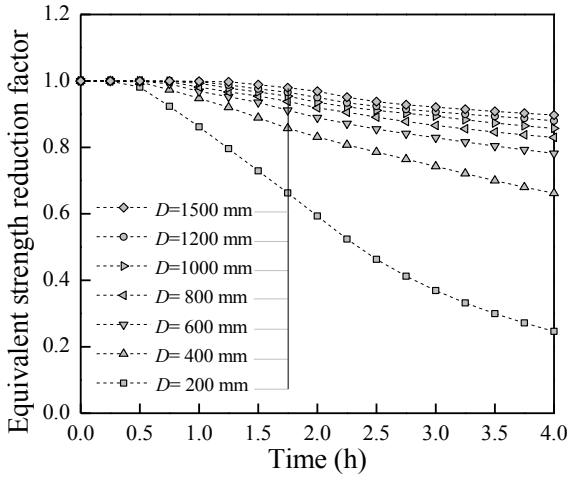

(a) Equivalent strength reduction factor

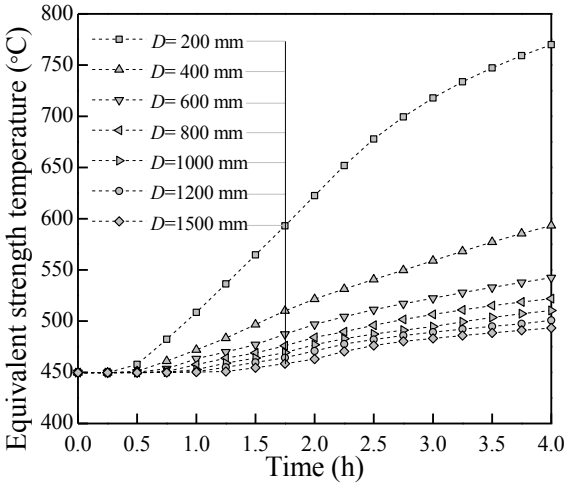

(b) Equivalent strength temperature

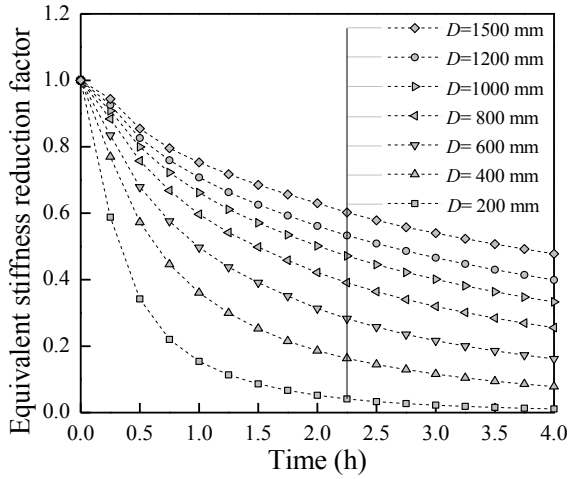

(c) Equivalent stiffness reduction factor

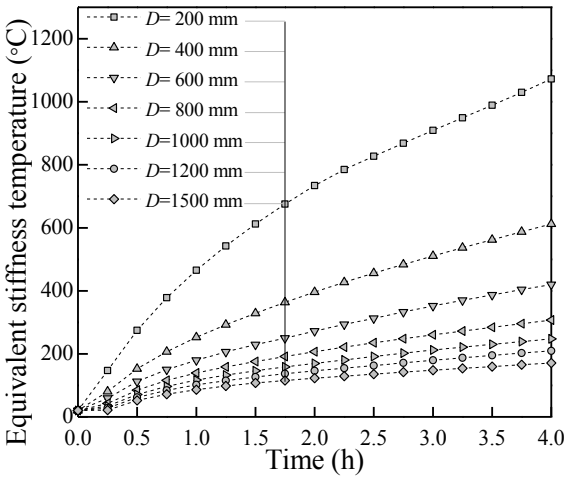

(d) Equivalent stiffness temperature

Fig. 17. Equivalent reduction factors and equivalent temperatures of the concrete core in unprotected square TRC sections

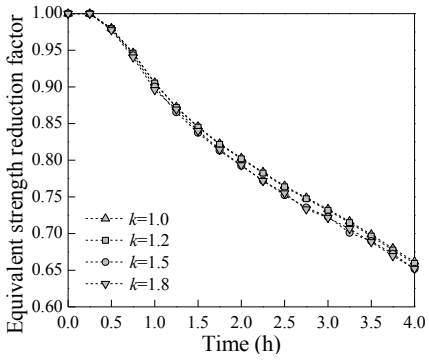

(a) k_{cfT} (D_{eq}=400 mm)

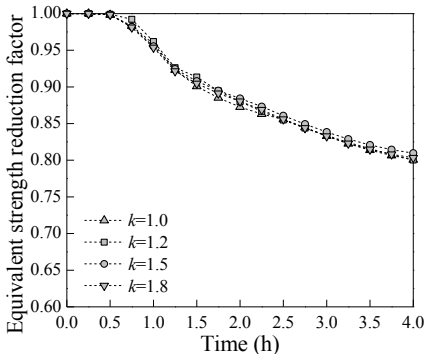

(b) k_{cfT} (D_{eq}=800 mm)

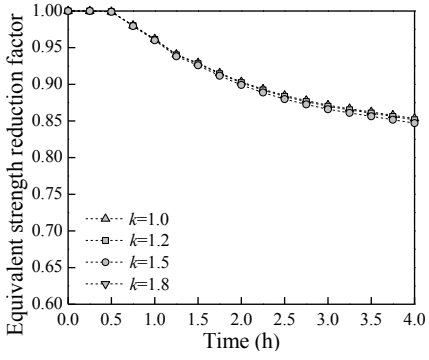

(c) k_{cfT} (D_{eq}=1000 mm)

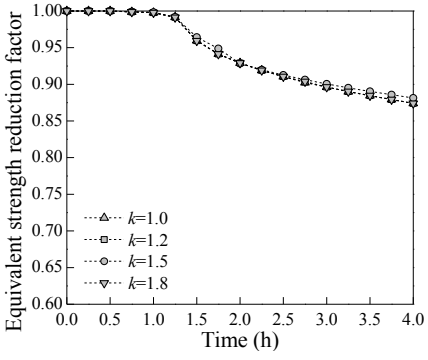

(d) k_{cfT} (D_{eq}=1500 mm)

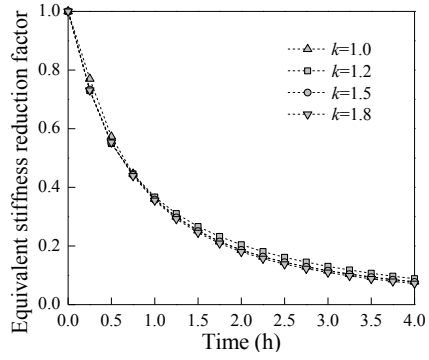

(e) k_{cET} (D_{eq}=400 mm)

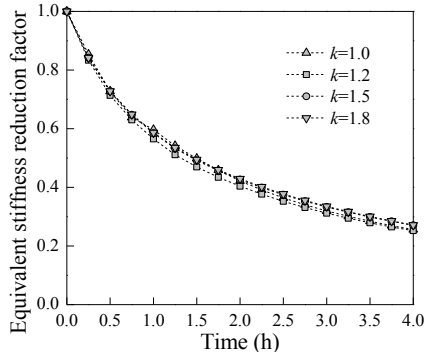

(f) k_{cET} (D_{eq}=800 mm)

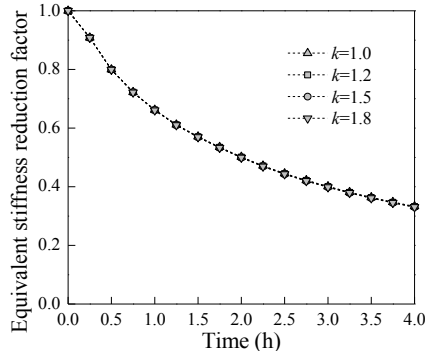

(g) k_{cET} (D_{eq}=1000 mm)

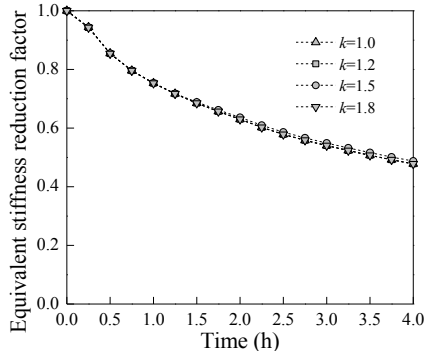

(h) k_{cET} (D_{eq}=1500 mm)

Fig. 18. Equivalent strength and stiffness reduction factors of the concrete core in unprotected rectangular TRC sections

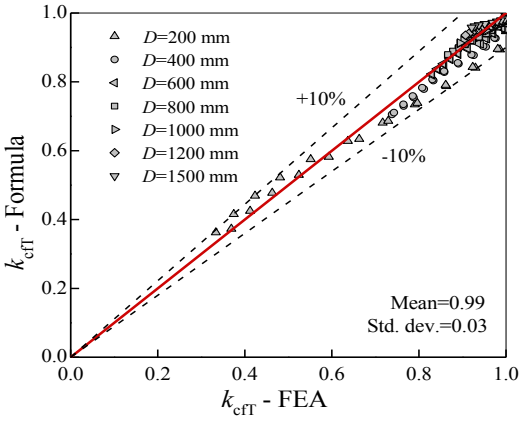

(a) Equivalent strength reduction factor

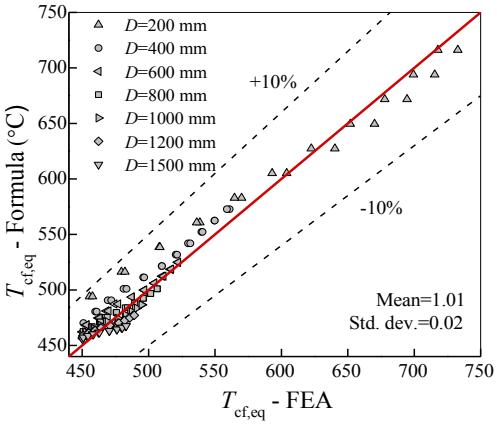

(b) Equivalent strength temperature

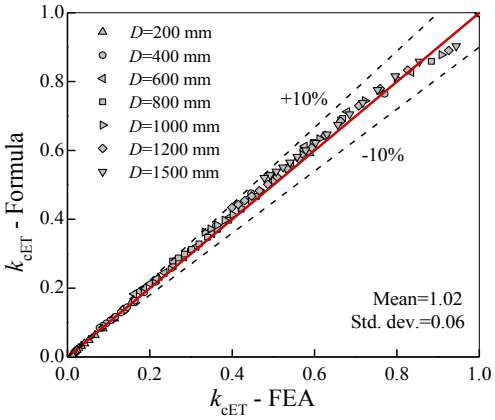

(c) Equivalent stiffness reduction factor

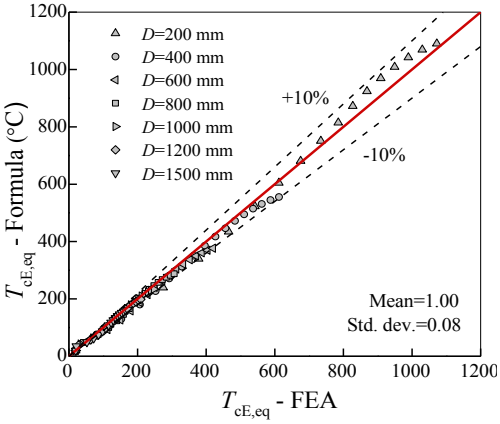

(d) Equivalent stiffness temperature

Fig. 19. Comparisons between the calculated equivalent reduction factors and equivalent temperatures with the FEA extracted ones

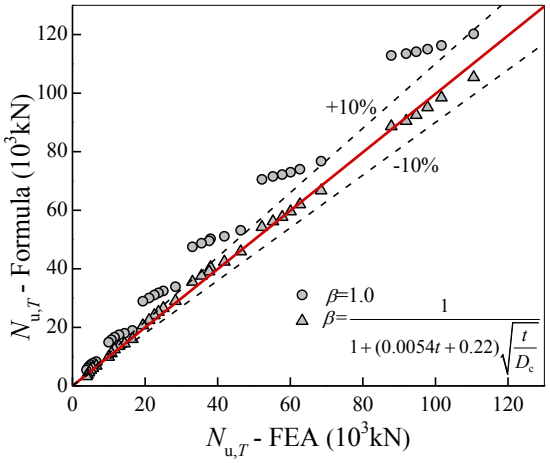

(a) Compressive resistance (square TRC)

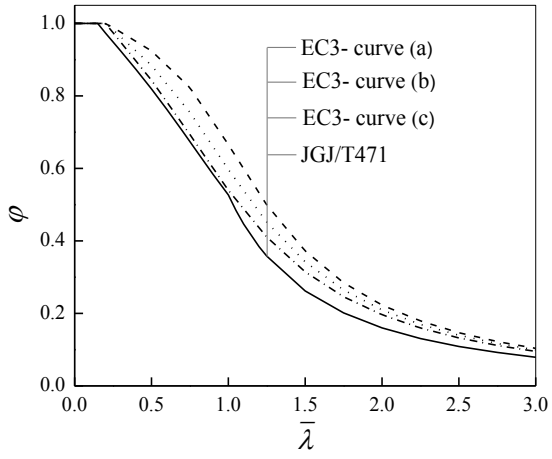

(b) Buckling curves

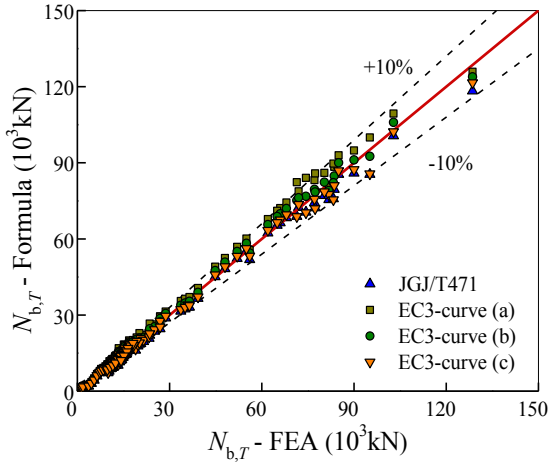

(c) Buckling resistance (square TRC)

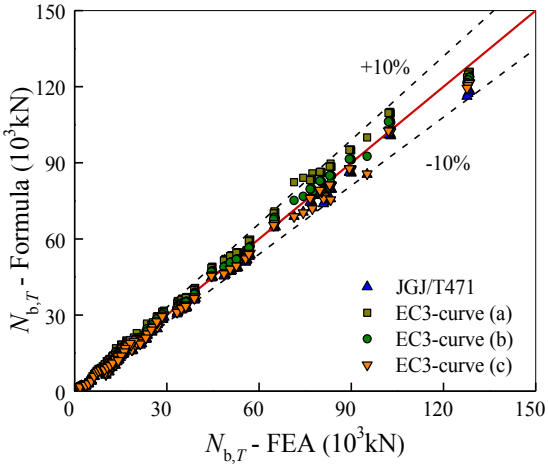

(d) Buckling resistance (rectangular TRC)

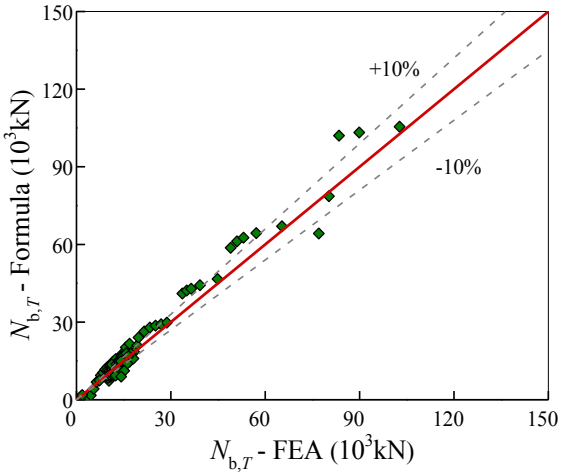

(e) New Annex H EN 1994-1-2 method (square TRC)

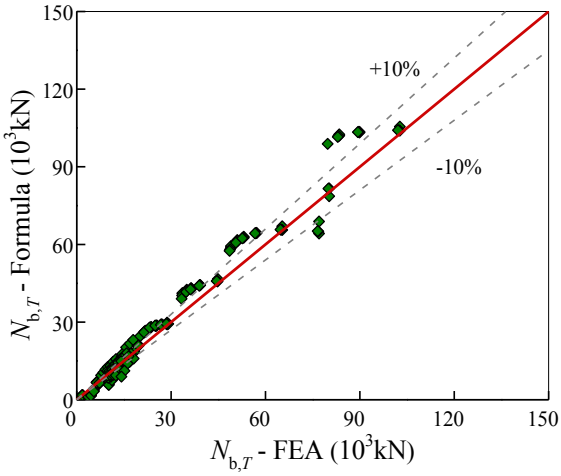

(f) New Annex H EN 1994-1-2 method (rectangular TRC)

Fig. 20. Compressive resistance and buckling resistance of square and rectangular TRC columns

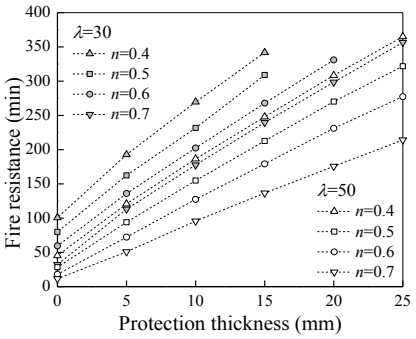

(a) D=200 mm

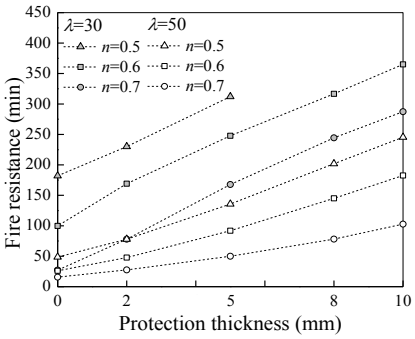

(b) D=400 mm

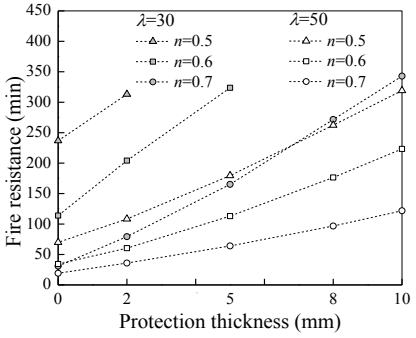

(c) D=600 mm

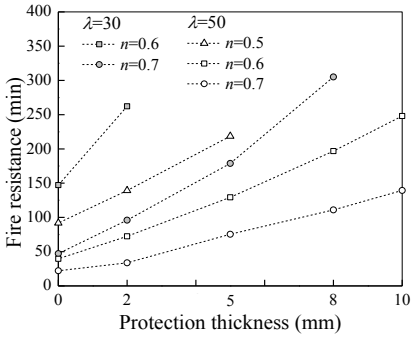

(d) D=800 mm

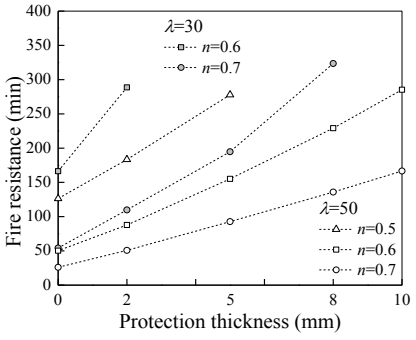

(e) D=1000 mm

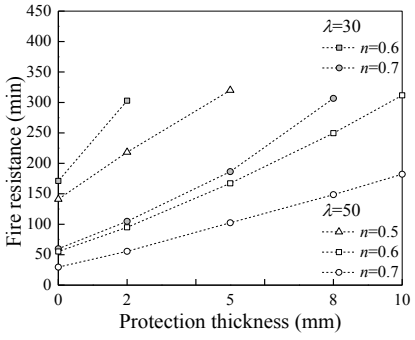

(f) D=1200 mm

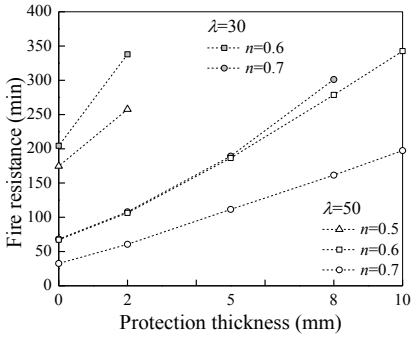

(g) D=1500 mm

Fig. 21. Influence of protection thickness on the fire resistance of protected square TRC columns

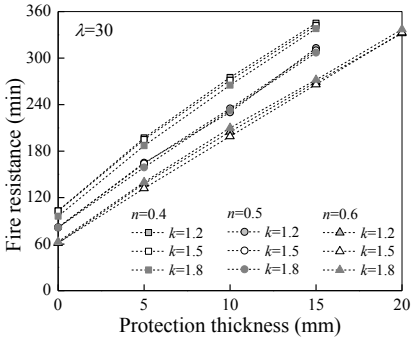

(a) D_{eq}=200 mm

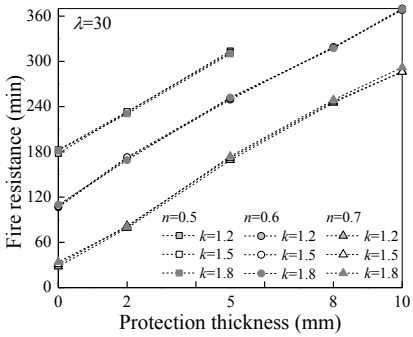

(b) D_{eq}=400 mm

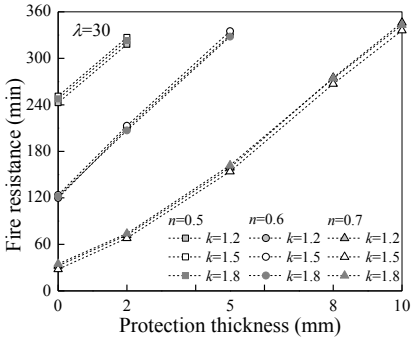

(c) D_{eq}=600 mm

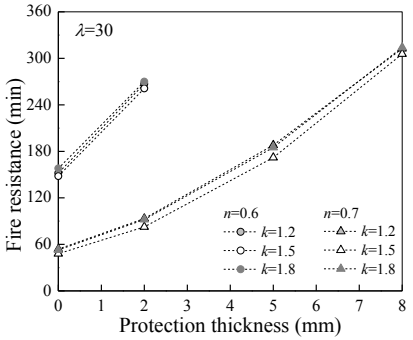

(d) D_{eq}=800 mm

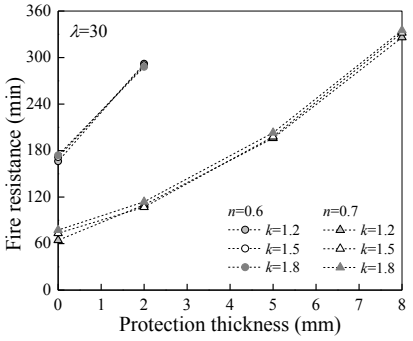

(e) D_{eq}=1000 mm

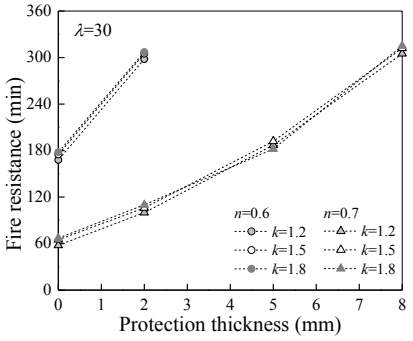

(f) D_{eq}=1200 mm

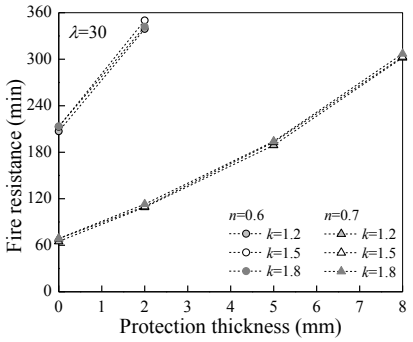

(g) D_{eq}=1500 mm

Fig. 22. Influence of protection thickness on the fire resistance of protected rectangular TRC columns

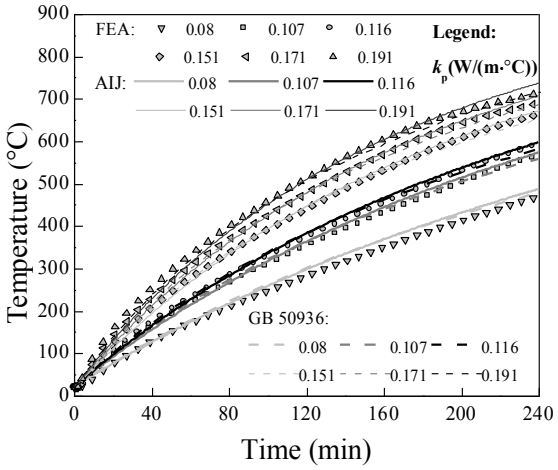

(a) Steel tube (different k_p)

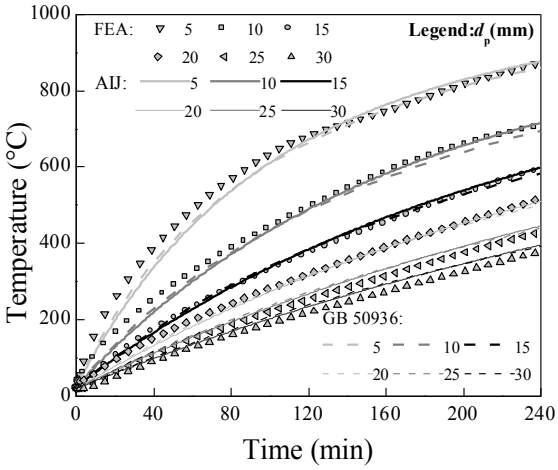

(b) Steel tube (different d_p)

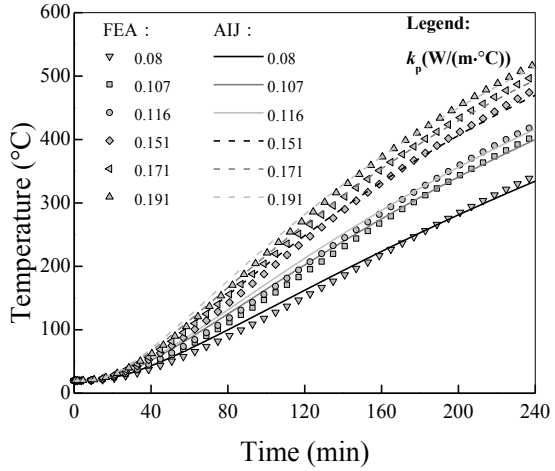

(c) Middle rebars (different k_p)

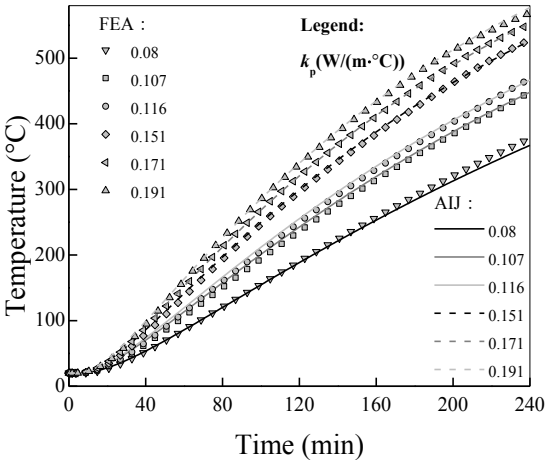

(d) Corner rebars (different k_p)

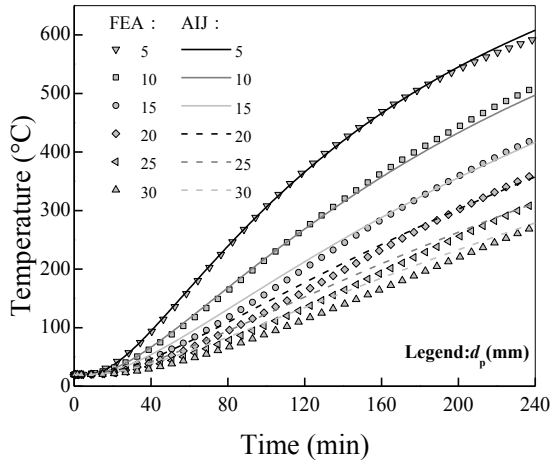

(e) Middle rebars (different d_p)

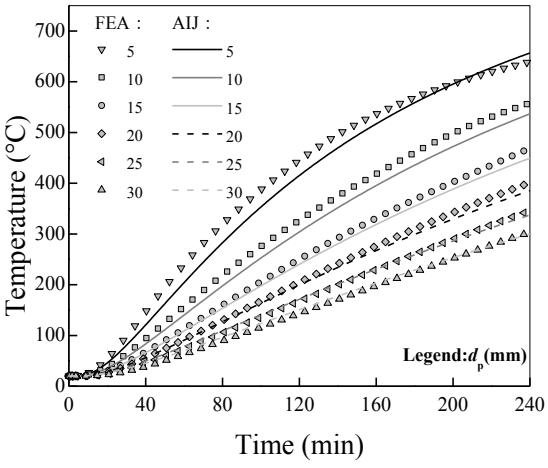

(f) Corner rebars (different d_p)

Fig. 23. Formula calculated and FEA predicted temperatures of steel tube and rebars in protected square TRC columns (D=200 mm)

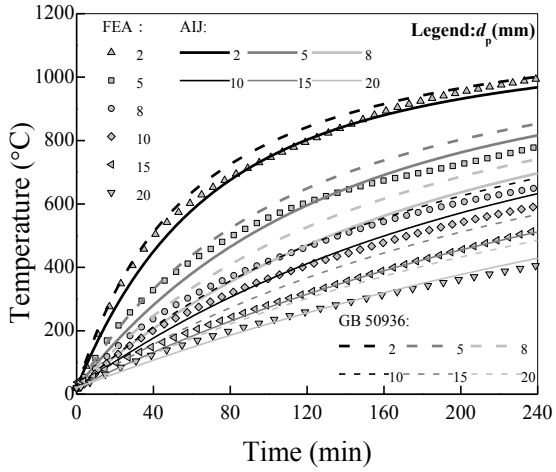

(a) Square TRC (D=400 mm)

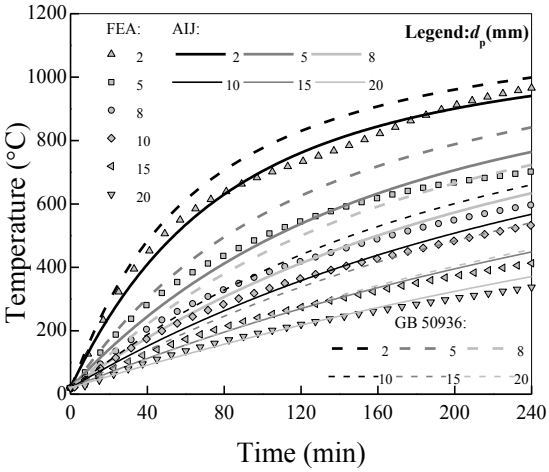

(b) Square TRC (D=800 mm)

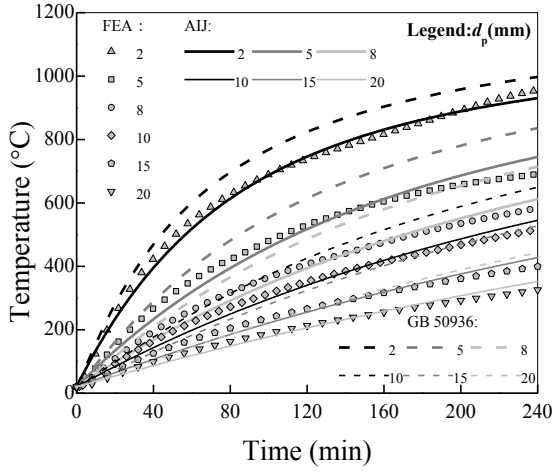

(c) Square TRC (D=1000 mm)

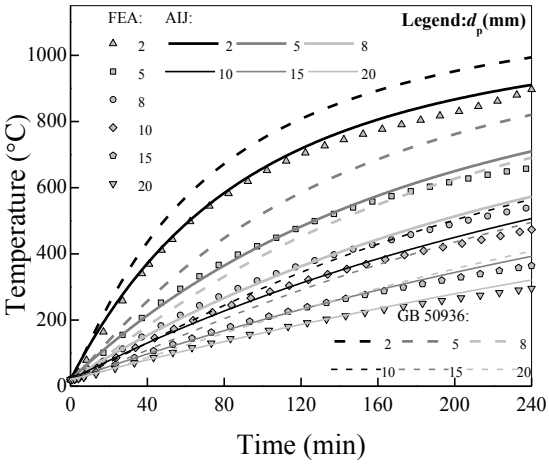

(d) Square TRC (D=1500 mmm)

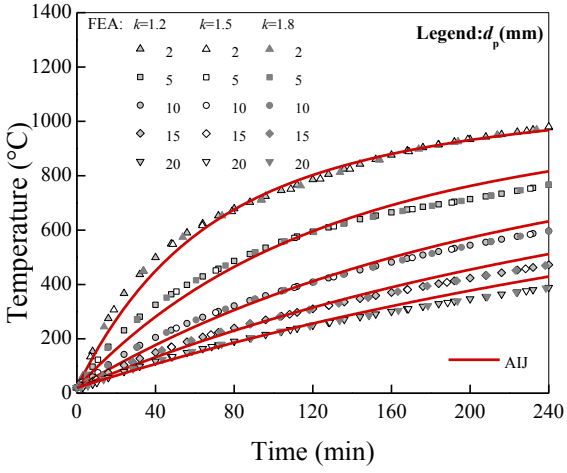

(e) Rectangular TRC (D_{eq}=400 mm)

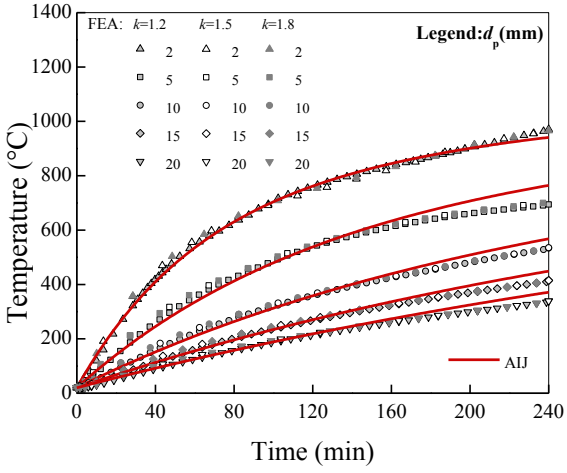

(f) Rectangular TRC (D_{eq}=800 mm)

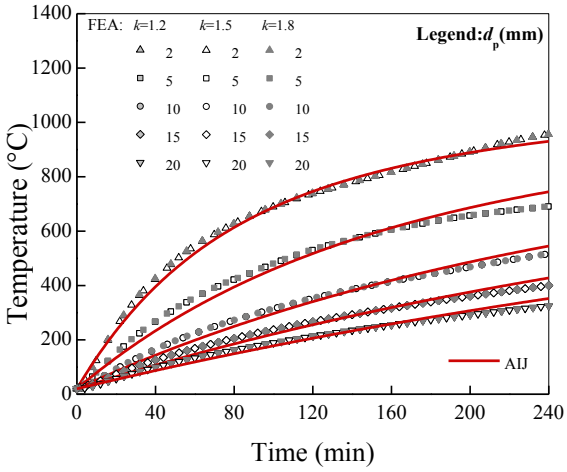

(g) Rectangular TRC (D_{eq}=1000 mm)

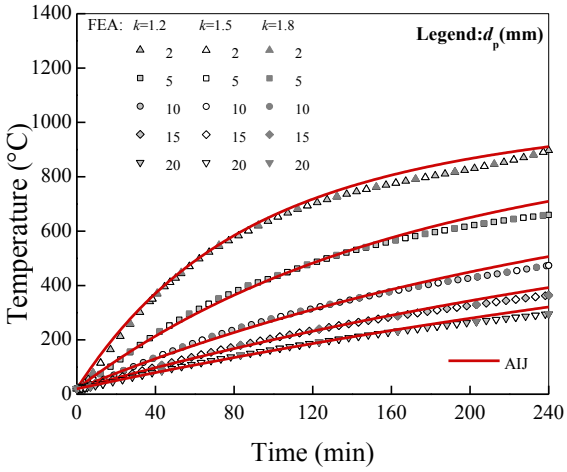

(h) Rectangular TRC (D_{eq}=1500 mm)

Fig. 24. Comparisons of the formula predicted steel tube temperatures and FEA ones for protected square and rectangular TRC columns

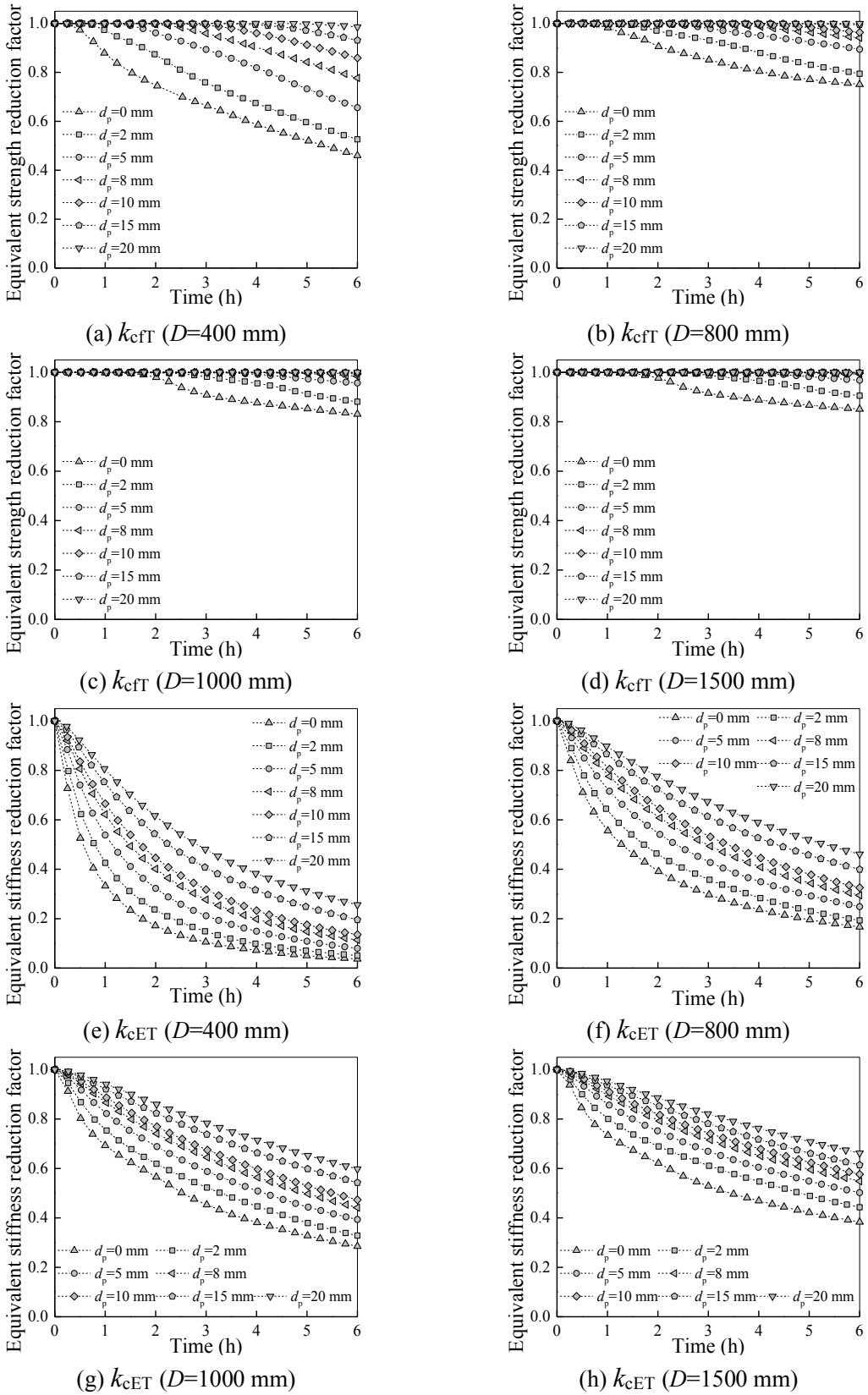

Fig. 25. Equivalent strength and stiffness reduction factors of the concrete core in protected square TRC sections

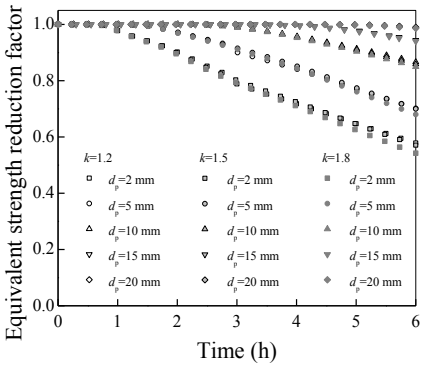

(a) k_{cfT} (D_{eq}=400 mm)

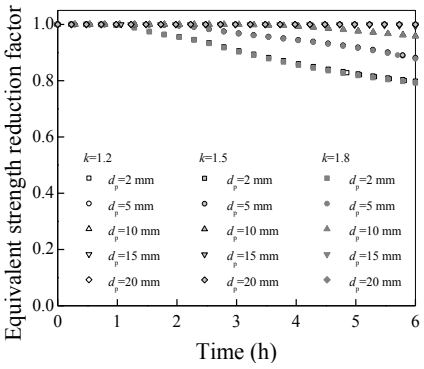

(b) k_{cfT} (D_{eq}=800 mm)

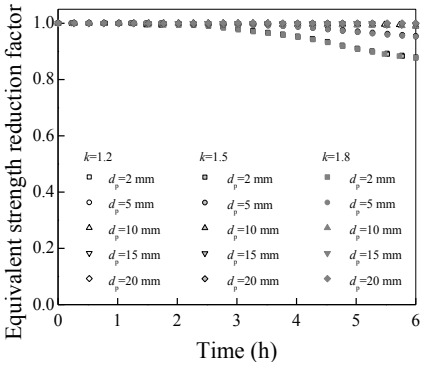

(c) k_{cfT} (D_{eq}=1000 mm)

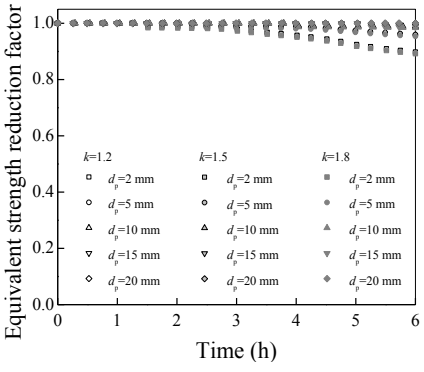

(d) k_{cfT} (D_{eq}=1500 mm)

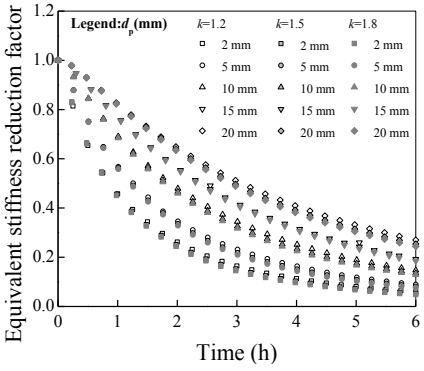

(e) k_{cET} (D_{eq}=400 mm)

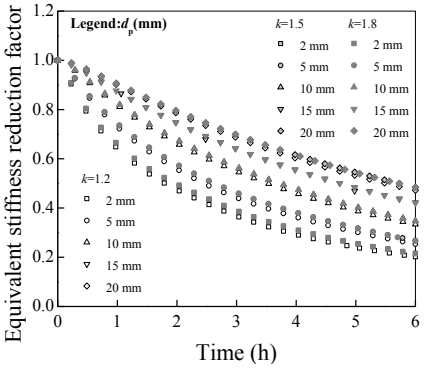

(f) k_{cET} (D_{eq}=800 mm)

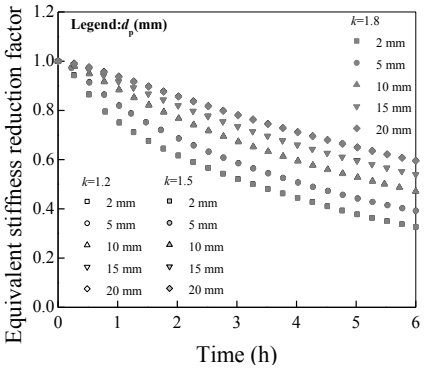

(g) k_{cET} (D_{eq}=1000 mm)

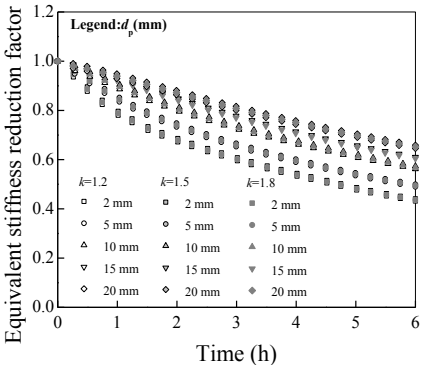

(h) k_{cET} (D_{eq}=1500 mm)

Fig. 26. Equivalent strength and stiffness reduction factors of the concrete core in protected rectangular TRC sections

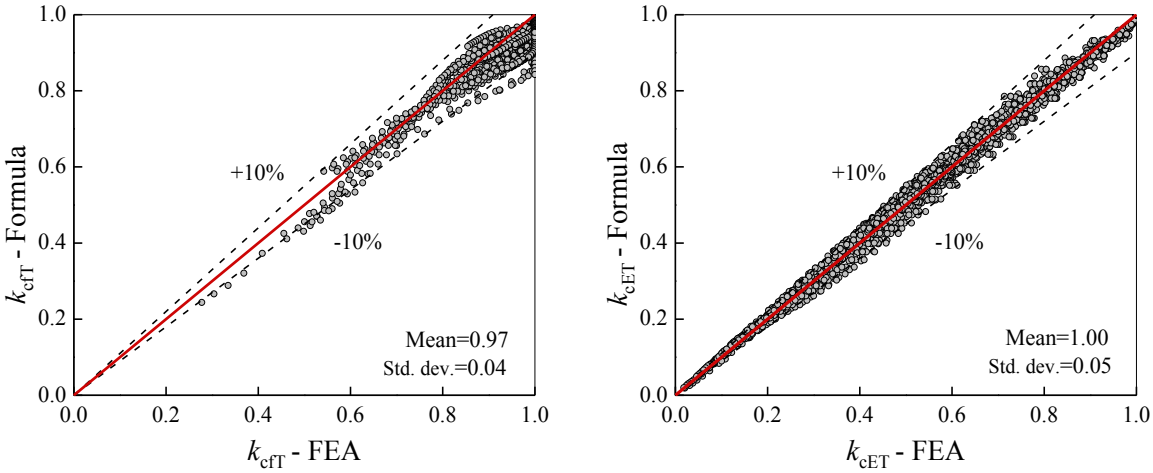

(a) Equivalent strength reduction factor

(b) Equivalent stiffness reduction factor

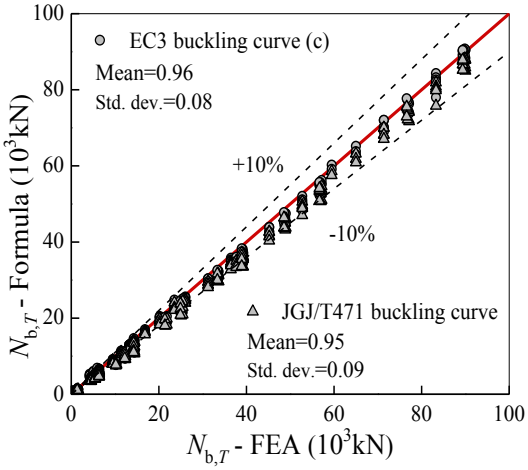

(c) Buckling resistance

Fig. 27. Comparisons between the calculated equivalent reduction factors and buckling resistance with the FEA ones for protected square and rectangular TRC columns

Table 1

Details of the tested rectangular TRC columns

Column No.	$D \times B$ (mm)		t_s (mm)		k	α_s	ρ	n	N_f	$t_{FR,t}$
	Nominal	Measured	Nominal	Measured		(%)	(%)		(kN)	(min)
TRC-0.5-1.5	250×167	251.3×167.5	2.20	2.20	1.5	4.55	2.79	0.5	1218.7	60.5
TRC-0.5-2	250×125	250.6×125.4	2.20	2.18	2.0	5.51	2.84	0.5	523.9	48.2

Table 2

Mechanical properties of steel tube and reinforcing bars at ambient temperature

Labels	ϕ or t_s (mm)	f_y or f_b (MPa)	f_u (MPa)	E_s or E_b (10^5MPa)	v
Rebar-16	15.65	441.33	626.41	2.05	0.29
Rebar-14	13.47	467.95	650.82	1.99	0.28
Rebar-12	11.23	517.18	746.31	2.03	0.29
Stirrup-10	9.87	361.00	574.96	2.09	0.30
Stirrup-8	7.95	343.25	562.17	2.04	0.30
Steel tube	2.07	280.72	442.94	2.06	0.30

Table 3

Collected fire test results of CFST and RC columns

Column type and No.		Section	D or $D\times B$ (mm)	t_s (mm)	$L(L_e)$ (m)	Reinf.	BC	f_y (MPa)	f_c' (MPa)	f_b (MPa)	d_p (mm)	N_f (kN)	$t_{FR,t}$ (min)	$t_{FR,p}$ (min)	$t_{FR,p}$/ $t_{FR,t}$
CFST	SQ-01	S	152.4	6.35	3.81(3.048)	-	F-F	350	58.3	-	0	376	66	67.1	1.02
Ref. [52]	SQ-02	S	152.4	6.35	3.81(3.048)	-	F-F	350	46.5	-	0	286	86	72.2	0.84
	SQ-07	S	177.8	6.35	3.81(3.048)	-	F-F	350	57	-	0	549	80	84.5	1.06
	SQ-20	S	254	6.35	3.81(3.048)	-	F-F	350	46.5	-	0	931	97	107.2	1.11
CFST	SQ-12	S	203.2	6.35	3.81(3.048)	4ϕ16	F-F	350	47	400	0	500	150	143.3	0.96
Ref. [53]	SQ-13	S	203.2	6.35	3.81(3.048)	4ϕ16	F-F	350	47	400	0	930	105	89.9	0.86
	SQ-18	S	254	6.35	3.81(3.048)	4ϕ19.5	F-F	350	48.1	400	0	1440	113	112.5	1.00
	SQ-19	S	254	6.35	3.81(3.048)	4ϕ19.5	F-F	350	48.1	400	0	2200	70	82.1	1.17
	SQ-22	S	304.8	6.35	3.81(3.048)	4ϕ16+4ϕ19.5	F-F	350	47	400	0	3400	39	35.9	0.92
	SQ-23	S	304.8	6.35	3.81(3.048)	4ϕ25.2	F-F	350	47	400	0	2000	212	215.3	1.02
CFST	R-1	R	300×200	7.96	3.81(3)	-	P-P	341	49	-	0	2486	21	20.1	0.96
Ref. [54]	R-3	R	300×150	7.96	3.81(3)	-	P-P	341	49	-	0	1906	16	18.8	1.18
	RP-1	R	300×200	7.96	3.81(3)	-	P-P	341	49	-	13	2486	104	104.7	1.01
	RP-2	R	300×200	7.96	3.81(3)	-	P-P	341	49	-	20	2486	146	153.5	1.05
	RP-3	R	300×150	7.96	3.81(3)	-	P-P	341	49	-	13	1906	78	84.1	1.08
	RP-4	R	300×150	7.96	3.81(3)	-	P-P	341	49	-	22.6	1906	122	130.2	1.07
	SP-2	S	350	7.7	3.81(3)	-	P-P	284	18.7	-	11	2700	140	143.9	1.03
CFST	S3	S	150	8	3.18(3.04)	4ϕ12	P-P	452.7	43.2	548	0	404.29	32	28.2	0.88
Ref. [55]	S4	S	220	10	3.18(3.04)	4ϕ16+4ϕ10	P-P	560.3	42.4	527(ϕ16) 575.3(ϕ10)	0	882.9	54	41.7	0.77

Table 3 (cont'd) Collected fire test results of CFST and RC columns

Column type and No.		Section	D or $D\times B$ (mm)	t_s (mm)	$L(L_e)$ (m)	Reinf.	BC	f_y (MPa)	f_c' (MPa)	f_b (MPa)	d_p (mm)	N_f (kN)	$t_{FR,t}$ (min)	$t_{FR,p}$ (min)	$t_{FR,p}/t_{FR,t}$
CFST	R1	R	250×150	10	3.18(3.04)	-	P-P	428.3	37.9	-	0	650.8	19	22.1	1.17
Ref. [50]	R2	R	250×150	10	3.18(3.04)	4ϕ16	P-P	428.3	39.6	527	0	699.8	23	24.9	1.08
	R7	R	350×150	10	3.18(3.04)	-	P-P	474	42.5	-	0	928.9	30	31.7	1.06
	R8	R	350×150	10	3.18(3.04)	4ϕ16+4ϕ10	P-P	474	38.2	527(ϕ16) 575(ϕ10)	0	988.8	21	18.9	0.90
RC	Ⅰ-2	S	305	-	3.81(3.048)	4ϕ25.4	F-F	-	36.9	444	0	1333	170	147.9	0.87
Ref. [57]	I-3	S	305	-	3.81(3.048)	4ϕ25.4	F-F	-	34.2	444	0	800	218	209.5	0.96
	I-4	S	305	-	3.81(3.048)	4ϕ25.4	F-F	-	35.1	444	0	711	220	228.9	1.04
	I-6	S	203	-	3.81(3.048)	4ϕ19.1	F-F		42.3	442	0	169	180	152.8	0.85
	I-7	S	305	-	3.81(3.048)	4ϕ25.4	F-F	-	36.1	444	0	1067	208	176.2	0.85
	I-8	S	305	-	3.81(3.048)	4ϕ25.4	F-F		34.8	444	0	1778	146	125	0.86
	I-9	S	305	-	3.81(3.048)	4ϕ25.4	F-F	-	38.3	444	0	1333	187	150.7	0.81
	I-12	S	305	-	3.81(3.048)	4ϕ25.4	F-F	-	39.9	444	0	1778	216	176	0.82
	Ⅱ-4	S	305	-	3.81(3.048)	4ϕ25.4	F-F	-	52.9	444	0	1178	227	199.4	0.88
	Ⅱ-5	S	305	-	3.81(3.048)	4ϕ25.4	F-F	-	49.5	444	0	1067	234	205.4	0.88
	Ⅱ-6	S	305	-	3.81(3.048)	4ϕ25.4	F-F	-	46.6	444	0	1076	188	202.4	1.08
	Ⅱ-7	S	305	-	3.81(3.048)	4ϕ25.4	F-F	-	42.5	444	0	947	259	213.4	0.82
	Ⅱ-8	S	305	-	3.81(3.048)	8ϕ25.4	F-F	-	42.6	444	0	978	252	219	0.87
	Ⅱ-9	S	305	-	3.81(3.048)	8ϕ25.4	F-F	-	37.1	444	0	1333	225	166.8	0.74
	Ⅱ-10	S	406	-	3.81(3.048)	8ϕ25.4	F-F	-	38.8	444	0	2418	262	301.3	1.15
	Ⅱ-11	S	406	-	3.81(3.048)	8ϕ32.3	F-F	-	38.4	414	0	2795	285	276.57	0.97
	Ⅲ-1	S	305	-	3.81(3.048)	4ϕ25.4	P-F	-	39.6	444	0	800	242	224.9	0.93
	Ⅲ-2	S	305	-	3.81(3.048)	4ϕ25.4	P-F	-	39.3	444	0	1000	220	215.2	0.98
	T-3	S	305	-	3.81(3.048)	4ϕ25.4	P-P	-	41.6	444	0	1022	221	193.7	0.88

Table 3 (cont'd) Collected fire test results of CFST and RC columns

Column type and No.		Section	D or $D\times B$ (mm)	t_s (mm)	$L(L_e)$ (m)	Reinf.	BC	f_y (MPa)	f_c' (MPa)	f_b (MPa)	d_p (mm)	N_f (kN)	$t_{FR,t}$ (min)	$t_{FR,p}$ (min)	$t_{FR,p}/t_{FR,t}$
RC	2	S	300	-	3.76	6ϕ20	P-P	-	24.1	487	0	930	84	101.2	1.08
Ref. [58]	3	S	300	-	3.76	6ϕ20	P-P	-	24.1	487	0	930	138	101.2	0.73
	5	S	300	-	4.76	6ϕ20	P-P	-	34.1	487	0	880	108	96.13	0.89
	7	S	300	-	5.76	6ϕ20	P-P	-	24.1	487	0	800	58	67.97	1.17
	8	S	200	-	3.76	4ϕ20	P-P	-	24.1	487	0	420	58	62	1.07
	9	S	200	-	3.76	4ϕ20	P-P	-	24.1	487	0	420	66	62	0.94
	10	S	200	-	3.76	4ϕ20	P-P	-	24.1	487	0	340	48	43	0.90

	Mean	0.97
	Std.dev.	0.12

Notes: "R" rectangular column; "S" square column; "D" sectional dimension of a square column or the depth of a rectangular column; "B" the width of a rectangular column; "t_s" thickness of steel tube; "ϕ" diameter of a reinforcing bar; "L" whole column length; "L_e" exposed column length; "BC" boundary condition; "P-P" pinned-pinned; "F-F" fixed-fixed; "P-F" pinned-fixed; "f_y" steel tube yield strength; "f_c'" concrete cylinder compressive strength; "f_b" reinforcing bar yield strength; "d_p" thickness of fire proof; "$t_{FR,t}$" tested fire resistance; "$t_{FR,p}$" predicted fire resistance.

Table 4

Investigated parameters in parametric studies of fire resistance

Parameters	Values	Defaut value
Load ratio n	0.4, 0.5, 0.6, 0.7,0.8	-
Dimension D (mm)	200, 400, 600, 800, 1000, 1200, 1500	600
Slenderness ratio (λ)	30,40,50,60	30
Concrete cube compressive strength f_{cu} (MPa)	30, 40, 50, 60	50
Steel tube yield strength f_y (MPa)	235, 345, 390, 420	345
Rebar yield strength f_b (MPa)	335, 400, 500	335
Steel ratio α_s (%)	2.0, 2.5, 3.0, 3.5, 4.0	3.0
Reinforcement ratio ρ (%)	2.0, 3.0, 4.0, 5.0, 6.0	4.0
Sectional aspect ratio k	1.0, 1.2, 1.5, 1.8	1.0